Acta Biomaterialia 202 (2025) 418–434

Contents lists available at ScienceDirect

Acta Biomaterialia

journal homepage: www.elsevier.com/locate/actbio

Full length article

In vitro and *in vivo* delivery of mRNA to joint cells using polymeric nanoparticles

Adriano P. Pontes [a], Jaqueline Lourdes Rios [b], Mattie Rijker [b], Kelly Warmink [b], Shreya Gudi [c], Francisco Conceição [c], Björn Meij [d], Tim J.M. Welting [e], Liliana Moreira Teixeira [c], Jaap Rip [a], Laura B. Creemers [b,*]

[a] *20Med Therapeutics B.V., Galileiweg 8, 2333 BD Leiden, the Netherlands*
[b] *Department of Orthopedics, University Medical Center Utrecht, Heidelberglaan 100, 3584 CX Utrecht, the Netherlands*
[c] *Department of Bioengineering Technologies, Technical Medical Centre, University of Twente, Drienerlolaan 5, 7522 NB Enschede, the Netherlands*
[d] *Department of Clinical Sciences, Faculty of Veterinary Medicine, Utrecht University, Yalelaan 108, 3584 CM, Utrecht, the Netherlands*
[e] *Laboratory for Experimental Orthopedics, Department of Orthopedic Surgery, Maastricht University, Maastricht, the Netherlands*

ARTICLE INFO

Keywords:
mRNA delivery
Chondrocyte
Organ-on-chip
Knee Joint
Osteoarthritis

ABSTRACT

Osteoarthritis (OA) is a progressive and degenerative disease of the joints, characterized by inflammation and loss of cartilage. Recently, mRNA therapies have emerged as promising disease-modifying treatments for cartilage repair and regeneration. Poly(amidoamine)-based polymeric nanoparticles (PAA-based NPs) were previously developed for intracellular mRNA delivery in chondrocytes, showing high biocompatibility and transfection efficiency. In this work, we aimed to evaluate this delivery system in models simulating the complex joint environment and *in vivo* in rat knee joints. For this purpose, cationic uncoated NPs and neutral PEG-coated NPs were formulated to test mRNA delivery in different models: (1) a 2D culture of chondrocytes supplemented with synthetic synovial fluid, (2) a cartilage-on-chip platform, (3) an *ex vivo* culture of mouse knee joints, and (4) an *in vivo* OA rat model. In the presence of synovial fluid, the PEG-coated NPs showed favorable physicochemical properties, higher cell uptake and equivalent GFP expression as uncoated NPs in the 2D cell culture. Similar observations were made using the cartilage-on-chip platform. In contrast, both NPs appeared to display cartilage penetration and uptake by tissue-resident chondrocytes in *ex vivo* joint culture. Upon intra-articular administration *in vivo*, the PAA-based NPs did not affect cartilage integrity in healthy nor OA rat knee joints, although enhanced synovial inflammation was observed. Uncoated NPs showed prolonged retention compared to PEG-coated NPs and higher luciferase expression in OA knee joints than in healthy joints of rats, whereas no difference was found for coated NPs. These results suggest that electrostatic interactions between cationic NPs and the anionic components of the extracellular matrix play a significant role in mRNA delivery to the articular cartilage, and that disease status may affect delivery of nucleic acids dependent on NP properties. In conclusion, PAA-based NPs are a promising platform for intra-articular mRNA delivery in the joints.

Statement of significance: In this study, we investigate the application of poly(amidoamine)-based polymeric nanoparticles (PAA-based NPs) for mRNA delivery in the joints, aiming for use in osteoarthritis (OA) treatment. The formulations were tested in *in vitro* models mimicking the joint environment, and also following intra-articular injection *ex vivo* and *in vivo* (OA-induced rats). We demonstrate for positively charged uncoated NPs higher *in vivo* gene expression in OA knee joints than neutral PEG-coated NPs. However, PEG-coated NPs induced more consistent gene expression in both healthy and OA knee joints. These findings highlight the potential of PAA-based NPs for osteoarthritis research and how the interplay between the NP properties, joint biology and disease state can affect mRNA delivery.

* Corresponding author at: Department of Orthopedics, University Medical Center Utrecht, Heidelberglaan 100, 3584 CX Utrecht, the Netherlands.
E-mail address: L.B.Creemers@umcutrecht.nl (L.B. Creemers).

https://doi.org/10.1016/j.actbio.2025.06.039
Received 14 March 2025; Received in revised form 3 June 2025; Accepted 22 June 2025
Available online 24 June 2025

1. Introduction

Osteoarthritis (OA) is a progressive musculoskeletal disorder affecting the synovial joints, commonly associated with ageing in conjunction with risk factors such as obesity and diabetes [1,2]. It is characterized by synovial inflammation and loss of articular cartilage, leading to severe pain and impaired mobility [2]. Globally, it affected over 500 million people in 2020 and estimates indicate that nearly 1 billion individuals will have OA in the year 2050, representing a major challenge to healthcare systems [3]. The available pharmacological therapies are based on pain control, including analgesic anti-inflammatory drugs (NSAIDs) [4], but their efficacy is relatively low due to the rapid clearance from the joints [5] and high incidence of side effects [6]. For most systemically administered drugs, the concentrations in the synovial fluid reach only 23–50 % of the levels found in the plasma [7]. Intra-articular therapy can maximize therapeutic efficacy in OA treatment, as it can achieve higher concentrations of drugs at the site of administration compared to systemic delivery [8].

Recently, nucleic acid-based approaches such as messenger RNA (mRNA)-delivering systems have shown great potential as a disease-modifying strategy for OA as an alternative to pharmacological therapies [9]. These mRNAs are often encapsulated in nanoparticle delivery systems for protection against degradation and optimal cell uptake [10]. The transient nature of mRNA is associated to a high safety profile, and in OA it offers the advantage of promoting the expression of transcription/epigenetic factors that act on cartilage repair [11]. The delivery of *Runx1* mRNA in polyamino acid nanomicelles [12] and of *Dnmt3b* mRNA in peptide-based polyplexes [13] suppressed disease progression and increased expression of anabolism and proliferation markers in OA mouse models. Alternatively, mRNA-based nanosystems were shown to block critical pro-inflammatory signaling in OA, such as the β-catenin/Wnt3a and the IL-1 pathways, by promoting the expression of natural antagonists that decreased chondrocyte apoptosis and suppressed expression of inflammatory cytokines [14,15].

Lipid-based nanoparticles (LNPs) and polymeric nanoparticles (PNPs) are commonly used for nucleic acid delivery to the cartilage due to their small size, enhanced stability and extended retention in the joints [16]. Despite the advantages of local delivery, nanoparticles must still overcome obstacles to successfully deliver therapeutic agents into the cartilage. The articular cartilage consists of chondrocytes embedded in an extracellular matrix (ECM) consisting of collagen type II fibers and proteoglycans, together forming an intricate and negatively charged meshwork [17]. With a pore size of 50–100 nm between collagen fibrils [18], the cartilage ECM poses an important barrier for full-depth penetration of NPs in the tissue. Therefore, physicochemical properties such as particle size, hydrophilicity and surface charge are critical quality attributes that influence cartilage targeting, penetration and retention within the joints [19]. In addition, NP interaction with synovial fluid components (*e.g.*, hyaluronic acid and plasma proteins) is often overlooked in literature, but may have a significant impact on the properties and function of nanoparticles within the joint [20]. In a recent study with poly(amidoamine) (PAMAM) dendrimers [21], a significantly higher uptake to cartilage tissue was observed under protein-free (PBS) conditions as compared to NPs subjected to protein adsorption (incubation with synovial fluid from OA patients). This effect results from the formation of a protein corona on small cationic nanocarriers, which may influence the diffusional transport of NPs and their fate in the joints, including the interplay between NPs and cells for endocytosis [22].

In this study, we tested the application of poly(amidoamine)-based polymeric nanoparticles (*i.e.*, polymeric scaffolded ps-PAAQ NPs), previously developed as bioreducible carriers for *in vivo* delivery of mRNA [23,24]. The cationic core of ps-PAAQ NPs allows for efficient condensation of nucleic acids in an aqueous buffer, and their biocompatible and biodegradable properties enable controlled release in the reducing conditions of the cytosol. Moreover, this polymeric delivery platform offers distinct advantages in terms of scalability and development speed (possibility to carry different types of nucleic acids), ease of formulation (one-step process without need of further purification) and the ability to be lyophilized [24]. We have recently shown that these cationic ps-PAAQ NPs loaded with EGFP mRNA were efficiently internalized into chondrocytes *in vitro* [25], and the coating with an anionic copolymer composed of poly-L-glutamic acid and polyethylene glycol ($PGA_{7.5k}$-PEG_{5k}) improved GFP translation [25] and mRNA thermostability [23]. Indeed, the principle of PEG shielding has been widely applied to enhance particle stability through steric repulsion, leading to higher delivery efficacy and tolerability [26]. Although these results are promising for joint disease treatment, the performance of ps-PAAQ NPs in the joint environment is unknown.

This work aimed to evaluate the intra-articular application of ps-PAAQ NPs by testing this delivery system in models mimicking the joint environment as well as their *in vivo* behavior. Uncoated and PEG-coated ps-PAAQ NPs loaded with a mixture of fluorescently labeled and non-labeled EGFP mRNA were synthesized and physically characterized after incubation with a synthetic synovial fluid. They were also compared in a 2D chondrocyte culture regarding uptake and GFP expression in the presence of synovial fluid. Nanoparticle diffusion and GFP protein expression were further tested in a cartilage-on-chip platform containing chondrocytes embedded in a 3D-collagen matrix. In addition, cartilage penetration and uptake by tissue-resident chondrocytes were tested in an *ex vivo* model of short-term incubation of mouse knee joints. Finally, ps-PAAQ NPs loaded with a mixture of fluorescently labeled and non-labeled luciferase mRNA were injected into healthy and OA-induced rat knee joints *in vivo*, in order to analyze local mRNA retention and translation over a period up to 4 weeks.

2. Materials and methods

2.1. Synthesis of the ps-PAAQ polymers

The ps-PAAQ (or p(CBA-ABOL-Q)/PEI) was synthesized and characterized by NMR and GPC as previously described [23,25]. The monomer of cystamine bis(acrylamide) (CBA) was synthesized as described by Lin *et al.* [27], while the monomer of N1-(7-chloroquinolin-4-yl)-hexane-1,6-diamine (Q6) was synthesized according to Natarajan *et al.* [28]. The CBA and quinoline-containing monomers were characterized by NMR and in agreement with previously published spectra [25]. Other chemicals were purchased and used without further purification from Sigma-Aldrich or Avantor. In brief, a mixture of the two amine-containing building blocks, 4-aminobutanol (ABOL) and Q6, were used to generate a random PAAQ co-polymer with the CBA. This Aza-Michael reaction takes place in a polar protic solvent (MeOH), followed by the addition of a $CaCl_2$ catalyst. After 48 h, oligomeric ethyleneimine (PEI800) was added in a one-pot reaction, yielding branched ps-PAAQ polymers.

2.2. Nanoparticle formulation and characterization

The ps-PAAQ polymer was mixed with EGFP mRNA (CleanCap®, TriLink Biotechnologies) in 10 mM Histidine 10 % Trehalose buffer (pH 6.5−7.0) to obtain nanoparticles. First the ps-PAAQ was dissolved at the desired concentration, then the mRNA solution was added 1:1 v/v to the cationic polymers. In all formulations of this study, the resulting polymer-to-mRNA ratio was 25:1 w/w. After mixing, the solution was incubated for at least 15 min at room temperature before storage in the -80°C freezer.

For *in vitro* experiments, the formulations were prepared at a concentration of 1.5 mg/mL of polymer to 60 μg/mL of mRNA. Regarding the mRNA content, the ps-PAAQ NPs were co-loaded with non-labeled EGFP mRNA and labeled AZDye647-EGFP mRNA (RiboPro) at a 9:1 w/w ratio for 2D-transfection analysis by flow cytometry. For the transfections in the cartilage-on-chip platform, the labeled mRNA was the AZDye568-EGFP mRNA (RiboPro).

For *ex vivo* experiments, the prepared formulations had a higher concentration (6 mg/mL of polymer and 240 μg/mL of mRNA). The ps-PAAQ NPs were co-loaded with non-labeled EGFP mRNA and labeled AZDye568-EGFP mRNA (RiboPro) at a 9:1 w/w ratio. As a negative control, we also used non-fluorescent ps-PAAQ NPs loaded with only luciferase mRNA (CleanCap®, TriLink Biotechnologies).

For *in vivo* experiments, the prepared formulations had three different concentrations: 5 mg/mL of polymer and 200 μg/mL of mRNA, 7.5 mg/mL of polymer and 300 μg/mL of mRNA, and 10 mg/mL of polymer and 400 μg/mL of mRNA. The ps-PAAQ NPs were co-loaded with non-labeled luciferase mRNA (Ethris) and labeled DY776-luciferase mRNA (Ethris) at a 9.67:0.33 w/w ratio. As a control, we also used ps-PAAQ NPs co-loaded with non-labeled EGFP mRNA (Ethris) and labeled DY776-luciferase mRNA (Ethris) at the same ratio above.

To obtain PGA-PEG-coated nanoparticles, the coating material ($mPEG_{5k}$-b-PLE_{50}, Alamanda Polymers) was added to the mRNA solution in the first step, which was then added to the polymer solution in the same mixing step, using a 1:1 coating to ps-PAAQ w/w ratio. These nanoparticles were designated "PEG-coated NPs" in this study, while their counterparts without PGA-PEG coating were named "uncoated NPs".

The resulting nanoparticle size was measured using Dynamic Light Scattering (DLS) in the Zetasizer Nano ZS90 (Malvern), with a 90-degree scattering optics. Samples were analyzed at a final concentration of 0.6 mg/mL in 10 mM Histidine 10 % Trehalose pH 6.5 (formulation buffer) or simulated synovial fluid pH 7.4 (Biochemazone™), using a 1:1 v/v dilution ratio. This synthetic synovial fluid is a sterile solution that simulates the components and pH of synovial fluid, including albumin, gamma-globulin, phospholipids and hyaluronic acid in a PBS solution. After mixing and incubating for 30 min at room temperature, the samples were loaded in a disposable low volume cuvette (ZEN0118, Malvern) for measurements. Zeta potential measurements were performed in the same formulation buffer using a DTS1070 disposable cuvette (Malvern). Results were analyzed in the Zetasizer software (version 7.13, Malvern).

2.3. Cell culture

The C28/I2 human chondrocyte cell line was cultured in growth medium composed of Dulbecco's modified Eagle's medium (DMEM GlutaMAX™, high glucose, pyruvate; Gibco), supplemented with 10 % v/v fetal bovine serum (FBS; Biowest), 100 units/mL penicillin and 100 μg/mL streptomycin (P/S; Gibco) at 37°C under a humidified 5 % CO_2 atmosphere. Medium changes were performed every 3 days and cells were passaged at 70–90 % confluency at a seeding density of 6,000 cells/cm^2 in 75 cm^2 T-flasks.

2.4. In vitro delivery of mRNA-loaded NPs in 2D culture

For the 2D transfection experiments, C28/I2 cells were seeded in 48 well-culture plates (20,000 cells/cm^2) in growth medium. Twenty-four hours after seeding the cells, the medium was replaced by the same volume of mRNA-loaded NPs diluted to the final concentration of 60 μg/mL for transfection (=2.4 μg/mL of mRNA), using serum-free DMEM without antibiotics, supplemented with 20 mM sterile HEPES buffer (Gibco). Alternatively, we also diluted the NPs in buffered DMEM with 10 % v/v simulated synovial fluid pH 7.4 (BZ183; Biochemazone™). Following transfection at 37°C for 3 h, the serum-free medium (with or without synovial fluid) was replaced by complete growth medium. After additional incubation for 21 h, microscopy and flow cytometry were performed. The bright field and fluorescence imaging of the 2D cell culture were performed using the ZOE Fluorescent Cell Imager (Bio-Rad) with a 20X objective.

2.5. Flow cytometry

Cells were trypsinized with trypsin-EDTA (0.25 %) per well and incubated for 3 min at 37°C. Then, DMEM with 10 % v/v FBS was added to each well and the cells were resuspended. The cell suspension was collected and centrifuged for 5 min at 500xg. The medium was aspirated, and the pellet was resuspended in FACS buffer (0.5 % BSA, 2 mM EDTA in DPBS) containing 0.25 μg/mL of DAPI solution (Thermo Scientific) for dead cell exclusion. The samples were transferred to a 96-well plate and kept refrigerated until measurement was performed in a MACSQuant® Analyzer 16 Flow Cytometer (Miltenyi Biotec). For DAPI detection, we used the 405 nm laser with 450/50 nm filter (V1 channel). For GFP detection, we used the 488 nm laser with 525/50 nm filter (B1 channel). For the AzDye647 dye (NP uptake), we used the 640 nm laser with 667/30 filter (R1 channel). Forward/side scatter were adjusted using untreated cells, and laser voltage was adjusted using single-labeled controls. Recording conditions were set to collect 10,000 live, single cell events per sample. Analysis was performed in the MACS Quantify software version 3.0 (Miltenyi Biotec).

2.6. In vitro delivery of mRNA-loaded NPs in a cartilage-on-chip model

2.6.1. Microfluidic chip fabrication

Micropatterned SU-8 master molds were produced as described elsewhere [29]. In brief, silicon wafers (Okmetic) were spin-coated with SU-8100 negative photoresist (Microchem). The SU-8 photoresist was patterned by exposure to UV light with a 365 nm longpass filter using an EVG 620 mask aligner (EVGroup). The patterned wafers were lastly developed in RER600 (Fujifilm). Microfluidic chips were produced by soft lithography using polydimethylsiloxane (PDMS). A 1:10 mixture of curing agent (Sylgard 184, Dow Corning) and PDMS pre-polymer was degassed and poured onto SU-8 molds. The PDMS was then cured at 65°C overnight. The following day, the patterned PDMS was peeled from the SU-8 wafer and cut to obtain single microfluidic chips. The central chamber inlets/outlets and the perfusion (media) inlets/outlets were punched with 1.5 and 1 mm Ø biopsy punchers, respectively. Each PDMS chip was then oxygen plasma-bonded (Cute plasma oven, Femto Science) to a cover slip and stored until further use. The final microfluidic chip thus consists of a central tissue chamber, two perfusion channels on either side of the tissue chamber, with evenly spaced pillars separating the tissue chamber from the perfusion channels. The day before seeding cells, microfluidic chips were placed in a 65°C oven overnight to increase chip hydrophobicity. Prior to cell seeding/hydrogel injection, chips were sterilized under UV light for 15 min.

2.6.2. Diffusion of NPs through empty collagen type I hydrogel ECM

A collagen type I hydrogel of 4 mg/mL was prepared by mixing chilled 10x PBS, 0.1 M NaOH, sterile water and Type I collagen (10.2 mg/mL FibriCol® Advanced BioMatrix). Ten μL of the hydrogel solution was pipetted per microfluidic chip and allowed to polymerize for 90 min in the incubator at 37°C. Uncoated and PEG-coated NPs were diluted to a final concentration of 60 μg/mL in serum-free DMEM with 20 mM HEPES. Sterile 3 mL syringes were filled up with 1 mL of NP/DMEM solution and 20G blunt-end Luer lock syringe needles (Darwin microfluidics) were attached to the syringes. Segments of Tygon S3 E-lab tubing (Saint-Gobain) were cut and sterilized by flushing with 70 % ethanol. The NP/DMEM containing syringes were fastened onto a syringe pump (Harvard Apparatus) followed by attachment of one end of the sterilized tubing to each syringe. The tubing was filled with the NP/DMEM solution by running the pump at 100 μL/min to avoid introducing air bubbles into the chip. After the hydrogel had polymerized, 4 μL of DMEM was pipetted into the perfusion channels of the chip. Thereafter, 90° bent PDMS couplers (Darwin microfluidics) were inserted into the free end of the tubing and then inserted into the inlets of the perfusion channels. Lastly, the NP/DMEM solution was perfused at 25 μL/h for 2 h. Images of the hydrogel-containing central tissue

chamber were obtained at 15-minute intervals. Image acquisition was performed on the EVOS AMG fluorescence microscope (Thermo Fisher Scientific) with a 10X objective, using the Texas Red LED cube at 100 % intensity to visualize the AZDye568 dye. The 2D images captured per timepoint were stacked and subsequently processed using the ImageJ software. Diffusion of NPs through the hydrogel was quantified by measuring the intensity of AZDye568 across time, over a fixed rectangular ROI of 0.6 mm length (total width of tissue chamber is 1.2 mm) starting at the tissue chamber side of the pillars of the microfluidic chip.

2.6.3. Live-dead assay to assess viability of C28/I2 cells after NP delivery

C28/I2 cells were cultured as described in *2.3.*, trypsinized to obtain a cell suspension and mixed with 4 mg/mL collagen type I hydrogel to obtain a final cellular concentration of 2,000,000 cells/mL. After sterilization, each chip was loaded with 10 μL of the hydrogel/cells mixture so that each chip had ≈20,000 cells. After allowing the hydrogel to polymerize as mentioned in *2.6.2.*, perfusion channels were filled up with 4 μL of serum-free buffered DMEM or buffered DMEM with 10 % v/v simulated synovial fluid. Next, uncoated and PEG-coated NP solutions containing non-labeled luciferase mRNA were prepared in DMEM or 10 % v/v synovial fluid to obtain a final mRNA concentration of 2.4 μg/mL. This was followed by filling up sterile 3 mL syringes with NP/ DMEM or 10 % v/v synovial fluid and setting up the syringes on the syringe pump with tubing as mentioned in *2.6.2.* Lastly, the NP/ DMEM or 10 % v/v synovial fluid solutions were perfused through the perfusion channels at 25 μL/h for 3 h. After 3 h perfusion was halted, and the hydrogel embedded cells were cultured statically in the microfluidic device for 21 h. For each condition, a representative chip ($n = 1$) was perfused, and each chip was imaged at three different locations (technical replicates = 3). After 21 h of static culture, cells in the microfluidic device were stained with Calcein AM (1:1000 in PBS) and Ethidium homodimer (1:500 in PBS) (Invitrogen) for 30 min and imaged using a confocal microscope to quantify cell viability.

2.6.4. In vitro delivery of mRNA-loaded NPs for transfection efficiency analysis

C28/I2 cells were embedded in 4 mg/mL collagen hydrogel and seeded in the microfluidic chip and as mentioned in *2.6.3.* Next, uncoated and PEG-coated NPs containing AZDye568-EGFP mRNA were diluted in DMEM or 10 % v/v synovial fluid to obtain a final mRNA concentration of 2.4 μg/mL. The NP/ DMEM or 10 % v/v synovial fluid solutions were then perfused at 25 μL/h for 3 h. After 3 h perfusion was halted, and the hydrogel embedded cells were cultured statically in the microfluidic device for 21 h to allow time for GFP expression. For each condition, three chips were perfused ($n = 3$) and each chip was imaged in 3D at three different positions (technical replicates = 3), corresponding to 800–1100 cells per condition. After 21 h of static culture, nuclei were stained with Hoechst (BioRad) by diluting 1:2000 in PBS for 30 min. Finally, the samples were imaged using a confocal microscope to analyze NP entry into the hydrogel and GFP expression.

2.6.5. Confocal microscopy for characterization of NP entry, GFP expression and live-dead assay post perfusion

Cell viability, NP entry and GFP expression were assessed using a confocal microscope (Zeiss LSM 880) equipped with a 10X air objective lens (0.3 NA). Hoechst staining was detected with 405 nm excitation and a 430–480 nm emission filter. The AzDye568 (NP uptake) and ethidium homodimer were imaged using 561 nm excitation and a 580–690 nm emission filter. GFP and Calcein AM fluorescence were detected with 488 nm excitation and a 500–550 nm emission filter. A pinhole size of 1 Airy unit was set for optical sectioning and Z-stacks were captured with a 3 μm step size over a total sample thickness ranging from 60–200 μm, which varied due to variations in the hydrogel heights post polymerization. 3D images per location on the microfluidic chip were stacked using the Maximum Intensity Projection algorithm and consistently adjusted for brightness and contrast. Manual thresholding was applied to count Hoechst-positive cells, Ethidium homodimer-positive cells and GFP or Calcein AM-positive cells. Images were processed and analyzed using ImageJ software. Negative controls perfused with DMEM or 10 % v/v synovial fluid solutions (without NPs) were used to set background fluorescence levels.

2.7. Ex vivo delivery of mRNA-loaded NPs in mouse knee joints

2.7.1. Intra-articular injection of NPs with EGFP mRNA

The knee joints ($n = 10$) used for this experiment were collected from 5 surplus male, skeletally mature C57BL/6 mice (>16 weeks old) that were euthanized in the course of non-OA-related experiments at the Central Laboratory Animal Research Facility (GDL) of the Utrecht University. The animals were hereby reused instead of sacrificing extra mice, according to the "3Rs principle" for animal research. Each joint was considered as an individual replicate. For every experimental group, 4 knee joints were injected with NPs loaded with fluorescently labeled EGFP mRNA (uncoated or PEG-coated). As negative control PEG-coated NPs loaded with luciferase mRNA only ("non-fluorescent NPs") were injected (=2 knee joints). Injections were performed up to 4 h after the sacrifice of animals in a randomized, blinded manner. Before starting, the joints were disinfected with 70 % ethanol and the knees were shaved with a blade. For intra-articular delivery, 5 μL of the NP formulations (=1.2 μg of mRNA / 30 μg of NPs) was injected into each knee joint with a Hamilton syringe (29G needle, 100 μL syringe volume). After waiting for 10 seconds without releasing the plunger and removing the syringe, the joints were gently flexed and extended several times to ensure even distribution of the NPs. Before the next steps, the femur and the tibia were cut halfway using a bone cutter and scissors to isolate the joints, and the skin was removed with a scalpel and tweezers. The dissected joints were washed with PBS supplemented with 200 U/mL of penicillin and 200 mg/mL of streptomycin. Then they were placed in 15 mL Falcon tubes (1 joint per tube) containing 10 mL of DMEM supplemented with 200 U/mL of penicillin, 200 mg/mL of streptomycin and 2 mg/mL gentamicin, and incubated at 37°C under a humidified 5 % CO_2 atmosphere for 24 h.

2.7.2. Processing of mouse knee joints

After incubation, the joints were washed again with PBS the soft tissues around the joint and the bones were removed, and the joints were incubated in 4 % paraformaldehyde for fixation. This step was conducted at 4°C for 24 h. Fixed joints were washed with PBS and placed in 15 mL Falcon tubes with 0.5 M EDTA solution (pH 8.0) for decalcification, at 4°C under gentle agitation for 72 h. The decalcified joints were embedded in Tissue-Tek® O.C.T. compound (Sakura) with the patella facing down, using Peel-A-Way embedding molds (Sigma-Aldrich) on dry ice. After complete fixation to the mold, the ice blocks were wrapped in aluminum foil and stored in the -80°C freezer. Cryosectioning was performed in a cryostat (CryoStar NX70; Thermo Scientific), by cutting 20 μm-thick tissue sections of the whole joint (from the patella to the posterior portion) and collecting them sequentially on glass slides (3 sections per slide). After brief resting at room temperature, the slides were stored at -20°C protected from light. Finally, mounting and nuclear staining were done in a single step using ProLong™ Glass Antifade Mountant with NucBlue Stain (Thermo Fisher), according to the supplier's protocol, which contains the nuclear counterstain Hoechst 33342 to detect DNA.

2.7.3. Image acquisition and processing

The bright field and fluorescent imaging of the cartilage sections were performed using a confocal laser microscope (SPX8; Leica) and 63x/1.4 oil-immersion objective. The AZDye568-EGFP mRNA used as a tracker for the nanoparticles in the cartilage was visualized using a 554 nm excitation wavelength, while Hoechst 33342 was visualized using a 405 nm laser line. The Z-stacking method, changing the focal length from the bottom to the top of a tissue section, was used to provide an

orthogonal view of the tissue thickness as evidence of NP internalization. Image processing was conducted using ImageJ (version 1.53; National Institutes of Health). The composite images were obtained by combining 10 images of a stack taken at different focal distances, using the Maximum Intensity Projection algorithm (Z Project → Max Intensity).

2.8. In vivo delivery of mRNA-loaded NPs in rats

2.8.1. Animal model and experimental design

Animal care and experimental procedures were performed in agreement with the ARRIVE guidelines and the Dutch Law of Animal Experimentation, and approved by the Animal Ethics Committee in Utrecht, the Netherlands (#AVD11500202114837). Twenty-six female, 12 weeks old, Sprague–Dawley rats (RRID:RGD_70508; Charles River Laboratories International, Inc.; RRID:SCR_003792) were housed in groups under standard laboratory conditions (open cage, *ad libitum* food and water). Preoperatively (at least 30 minutes prior surgery), rats received 0.03 mg/kg of buprenorphine (Temgesic®) and 4 mg/kg of carprofen (Carporal®) subcutaneously as prophylactic analgesia, and pre-operative antibiotics (10 mg/kg Enrofloxacin). Eight hours after first injection, they received another dose of buprenorphine. On days 1 and 2 post-surgery, all animals received another dose of carprofen. OA was induced by unilateral transection of the anterior cruciate ligament (ACL) and resection of the anterior horn of the medial meniscus, referred to as the anterior cruciate ligament transection combined with partial medial meniscectomy (ACLT + pMMx) model. This surgery was performed in the right knee of all rats under isoflurane anesthesia (4–5 % for induction; 1.5–3 % for maintenance). The left knees were used as healthy controls and did not receive OA induction surgery. After 4 weeks, a volume of 25 µl of ps-PAAQ NPs with different mRNA concentrations in buffer solution (10 % trehalose 10 mM histidine, pH 7) was injected intra-articularly through the patellar tendon in a flexed knee, using insulin syringes (30G, BD Micro-Fine). A preliminary pilot study was performed to assess possible adverse reactions of the injection of ps-PAAQ NPs in the rats. Rats were randomly divided and for every combination of NP type (uncoated or PEG-coated) and disease state (healthy and OA), 2 rats were injected with NPs loaded with luciferase mRNA and 2 rats were injected with NPs loaded with EGFP mRNA (10 µg mRNA doses). In a larger follow-up study examining NP retention and mRNA dose-dependent luciferase expression, animals were divided into 9 groups (each $n = 3$; negative control $n = 2$) that received in both knees intra-articular (IA) injections of either uncoated or PEG-coated NPs with mRNA at increasing concentrations as described in Table 1. Two additional rats did not receive NP injections nor OA surgery, serving as negative controls for correction of the fluorescent signal (see below). The nanoparticles were injected on days 0 and 7, respectively 4 and 5 weeks after the OA-inducing surgery. Both healthy and diseased knees were injected while the rats were anesthetized with 1.5–3 % isoflurane.

The injections and data analysis were done in a blinded manner. In the days following the first IA injection (days 1, 3, 5 and 7), the rats were imaged by near-infrared (NIR) and bioluminescence imaging (BLI). One week after the first IA injection, the rats received a second IA injection in both knees, followed by imaging (NIR and BLI) on days 8, 10, 12, 14, 21 and 28.

Table 1
Experimental groups and corresponding mRNA concentrations. All ps-PAAQ NPs were loaded with a mixture of non-labeled mRNA (luciferase or EGFP control) and fluorescently labeled luciferase mRNA (DY776 dye).

Group	Left/Healthy knee	Right/OA knee
Control mRNA uncoated ($n = 3$)	Uncoated NPs with 10 µg EGFP + DY776 mRNA	Uncoated NPs with 10 µg EGFP + DY776 mRNA
5 µg mRNA uncoated ($n = 3$)	Uncoated NPs with 5 µg luciferase + DY776 mRNA	Uncoated NPs with 5 µg luciferase + DY776 mRNA
7.5 µg mRNA uncoated ($n = 3$)	Uncoated NPs with 7.5 µg luciferase + DY776 mRNA	Uncoated NPs with 7.5 µg luciferase + DY776 mRNA
10 µg mRNA uncoated ($n = 3$)	Uncoated NPs with 10 µg luciferase + DY776 mRNA	Uncoated NPs with 10 µg luciferase + DY776 mRNA
Control mRNA PEG-coated ($n = 3$)	PEG-coated NPs with 10 µg EGFP + DY776 mRNA	PEG-coated NPs with 10 µg EGFP + DY776 mRNA
5 µg mRNA PEG-coated ($n = 3$)	PEG-coated NPs with 5 µg luciferase + DY776 mRNA	PEG-coated NPs with 5 µg luciferase + DY776 mRNA
7.5 µg mRNA PEG-coated ($n = 3$)	PEG-coated NPs with 7.5 µg luciferase + DY776 mRNA	PEG-coated NPs with 7.5 µg luciferase + DY776 mRNA
10 µg mRNA PEG-coated ($n = 3$)	PEG-coated NPs with 10 µg luciferase + DY776 mRNA	PEG-coated NPs with 10 µg luciferase + DY776 mRNA
Negative control ($n = 2$)	No NP injection	No NP injection

2.8.2. Histological staining and scoring

Left knees (healthy) and right knees (OA-induced) were harvested post-mortem. Knees were fixed in 10 % normal buffered formalin (NBF) for 1 week and then decalcified in 0.5 M EDTA (set to pH 7.0 with NaOH) for 6 weeks. Every week the samples were re-fixated in 10 % NBF for 24 h. In the end, knees were refixed in 10 % NBF and kept in NBF until further processing. The decalcified tissue was then dehydrated in a graded series of ethanol, cleared in xylene, and paraffin infiltrated. Knee joints were paraffin embedded in a 90°–100° angle with the patella facing down and then coronal sections (5 µm) at 200 µm intervals throughout the knee joint were made. Knee sections were deparaffinized and stained in two different manners for the Mankin and Kreen scoring. Sections were stained with Weigert's Hematoxylin, Fast Green and Safranin-O and the cartilage was evaluated using the Mankin score. The total Mankin score (0–56) is the sum of the subscores of the four cartilage compartments (tibia and femur, medial and lateral, 0–14). Sections were also stained with Mayer's Hematoxylin and Eosin (H&E) and the synovial inflammation was evaluated using the Krenn score [30]. All knees were scored in a blinded and randomized order. For each knee, the section at the 200 µm interval that looked the most damaged was scored.

2.8.3. Near infrared (NIR) imaging

To evaluate the presence of fluorescently labeled mRNA (DY776 dye) in the joints over time, *in vivo* imaging with Pearl® Impulse Small Animal Imager System (LICORbio) was performed on days 1, 3, 5, 7, 8, 10, 12, 14, 21 and 28. Animals were anesthetized with isoflurane (4–5 % for induction; 1.5–3 % for maintenance) and the knees were shaved to minimize scattering and absorption of light. Three images were acquired per subject (technical replicates), using the 800 nm and white light channels (85 µm resolution). The average from three scans were used to run the statistics.

Quantification of images was performed by using Pearl® Impulse Software (version 2, LICORbio). In brief, the total signal in the same ellipse of ±50,000 pixels was used to analyze the regions of interest in all rats. The background signal was measured using the negative control animals that were not operated and did not receive any IA nanoparticle injection (Table 1), and all data was corrected based on the mean background signal.

2.8.4. Bioluminescence imaging (BLI)

To evaluate the luciferase activity in the joints, BLI was performed on days 1, 3 and 8. Twenty minutes prior to BLI, rats were intraperitoneally injected with D-luciferin (MediLumine, 10 µL/g of body weight from a 15 µg/mL stock solution). The rats were imaged for protein expression for 5 min, using a Photon Imager (Biospace Lab). Quantification of data was done using M3 Vision software (Biospace Lab). Counts per minute were measured for both knees, and background signal was removed by subtracting the counts per minute from the abdominal region of the same rat, in an area of equivalent size to the area of the knee.

2.9. Statistics

Statistical analyses were performed using GraphPad Prism (version 9.3.1; GraphPad® Software). Normality of the data and residuals was checked using histograms and QQ plots. For the experiments with *in vitro* models, Two-Way ANOVAs followed by Tukey's test (2D culture) or by the Fisher's LSD test (cartilage-on-a-chip) were performed to determine how nanoparticle type and transfection medium affected cell uptake and GFP expression. The *in vivo* delivery of mRNA-loaded NPs to rat knee joints (NIR imaging) included repeated measures over time and was analyzed using a linear mixed model, followed by pairwise comparisons with Tukey's *post hoc* test. Bioluminescence imaging (BLI) results were analyzed using Two-Way ANOVA followed by Tukey's test, in order to determine how the experimental group and the mRNA concentration affected luciferase protein expression. Values of $p \leq 0.05$ were considered to be statistically significant. All data are shown as mean ± standard deviation.

3. Results

3.1. PEG coating maintains NP properties after incubation with synovial fluid

The synthesized ps-PAAQ polymers were formulated with EGFP mRNA to obtain nanoparticles designated "uncoated NPs". Alternatively, these polymers were co-formulated with EGFP mRNA and $PGA_{7.5k}$-PEG_{5k} to obtain nanoparticles designated "PEG-coated NPs". This specific PEG length (5k) was selected from a previous screening [23], showing the best properties for pharmaceutical formulations in terms of size distribution, surface change and stability. The DLS measurements confirmed the formation of nanoparticles. PEG-coated ps-PAAQ NPs showed an expected particle size around 50 nm and highly monodisperse distribution in formulation buffer (51.8 ± 1.1 nm; PDI 0.075 ± 0.018) (Fig. 1A). A larger hydrodynamic diameter was observed for uncoated NPs (101.8 ± 2.7 nm; PDI 0.202 ± 0.008). While incubation with synthetic synovial fluid did not affect the size of coated ps-PAAQ NPs (51.2 ± 3.1 nm; PDI 0.090 ± 0.038), it did promote a substantial increase in particle size for uncoated NPs (735.3 ± 59.1 nm; PDI 0.089 ± 0.078) (Fig. 1A).

The zeta potential showed near-neutral values for PEG-coated NPs in formulation buffer (−2.1 ± 0.4 mV), as an effect of the hydrophilic $PGA_{7.5k}$-PEG_{5k} addition, while uncoated NPs had a strongly positive zeta potential of +29.7 ± 0.7 mV (Fig. 1B). After incubation with synthetic synovial fluid, the coated ps-PAAQ NPs maintained the neutral zeta potential (−0.9 ± 0.7 mV), but uncoated NPs showed a substantial reduction in the positive surface charge and eventually became electroneutral (+0.4 ± 0.2 mV). The respective particle size distributions are shown in **Supplementary Fig. S1**, indicating that all groups are monodispersed as 100 % of the measurements fall within a single peak of intensity, even though a higher variability in peak size was found for NPs in synovial fluid (uncoated and coated). In previous work, cryo-EM was used to show shape and size of the NPs [25], and the successful coating was confirmed by comparing particle size and surface charge at different PGA-PEG to ps-PAAQ weight ratios [23]. The loading efficiency of mRNA in the NPs was previously characterized by gel electrophoresis and RiboGreen assay, showing nearly 100 % of encapsulation efficiency [23,25].

3.2. In vitro transfection of chondrocytes in the presence of synovial fluid affects NP uptake and GFP expression of uncoated NPs, but not of PEG-coated NPs

To evaluate the effect of the synovial fluid on the NP uptake and GFP expression, we used a 2D culture model consisting of C28/I2 chondrocytes in monolayer, a relevant cell type for testing the intra-articular application of our technology. The uncoated NPs were compared to the PEG-coated NPs, after loading them with a mixture of labeled (AZDye647) and non-labeled EGFP mRNA. The size distribution of these formulations is shown in **Supplementary Fig. S2**, demonstrating the differences between uncoated NPs (size 61.4 nm / zeta +35.7 mV) and PEG-coated NPs (size 40.3 nm / zeta −8.5 mV). For the transfection, we used a final concentration of 2.4 µg/mL of mRNA loaded in ps-PAAQ NPs diluted either in DMEM or in 10 % v/v synovial fluid. This dosage was previously shown by us to be well tolerated in C28/I2 cells (viability ≥95 %) [25]. The uptake efficiency and GFP expression were analyzed after 24 h by FACS and quantified by the percentage of positive cells and median fluorescence intensity (MFI). We previously investigated in more detail the uptake and intracellular trafficking of these NPs in C28/I2 cells transfected in FBS-free DMEM [25], but this is the first time we transfect them in the presence of synovial fluid.

Regarding the uptake efficiency (% of AZDye647-positive cells), Fig. 2A shows that in all conditions nearly 100 % of cells had

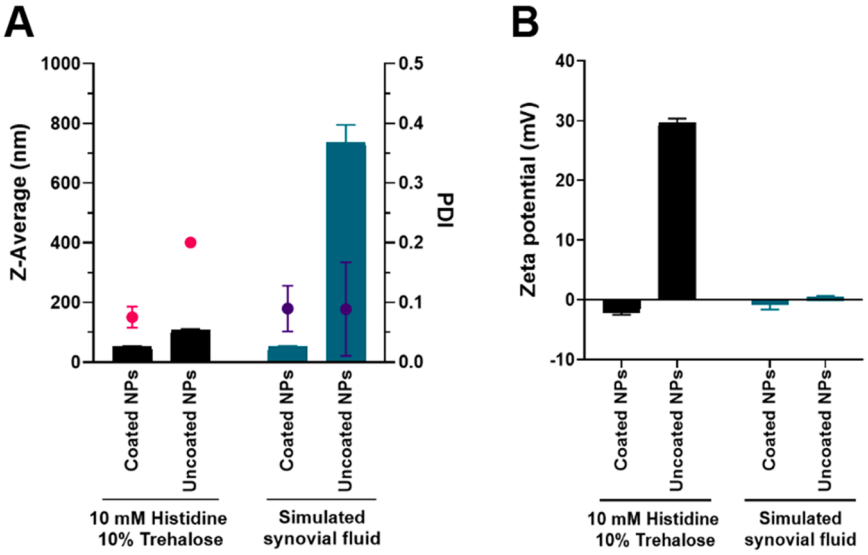

Fig. 1. Particle size **(A)** and zeta potential **(B)** after incubation of ps-PAAQ NPs with formulation buffer or simulated synovial fluid. All formulations were loaded with EGFP mRNA at a 25:1 w/w polymer-to-mRNA ratio. Bars represent Z-Average (in nm) or zeta potential (in mV) and dots represent polydispersity index (PDI). Results are the combined data of three individual measurements.

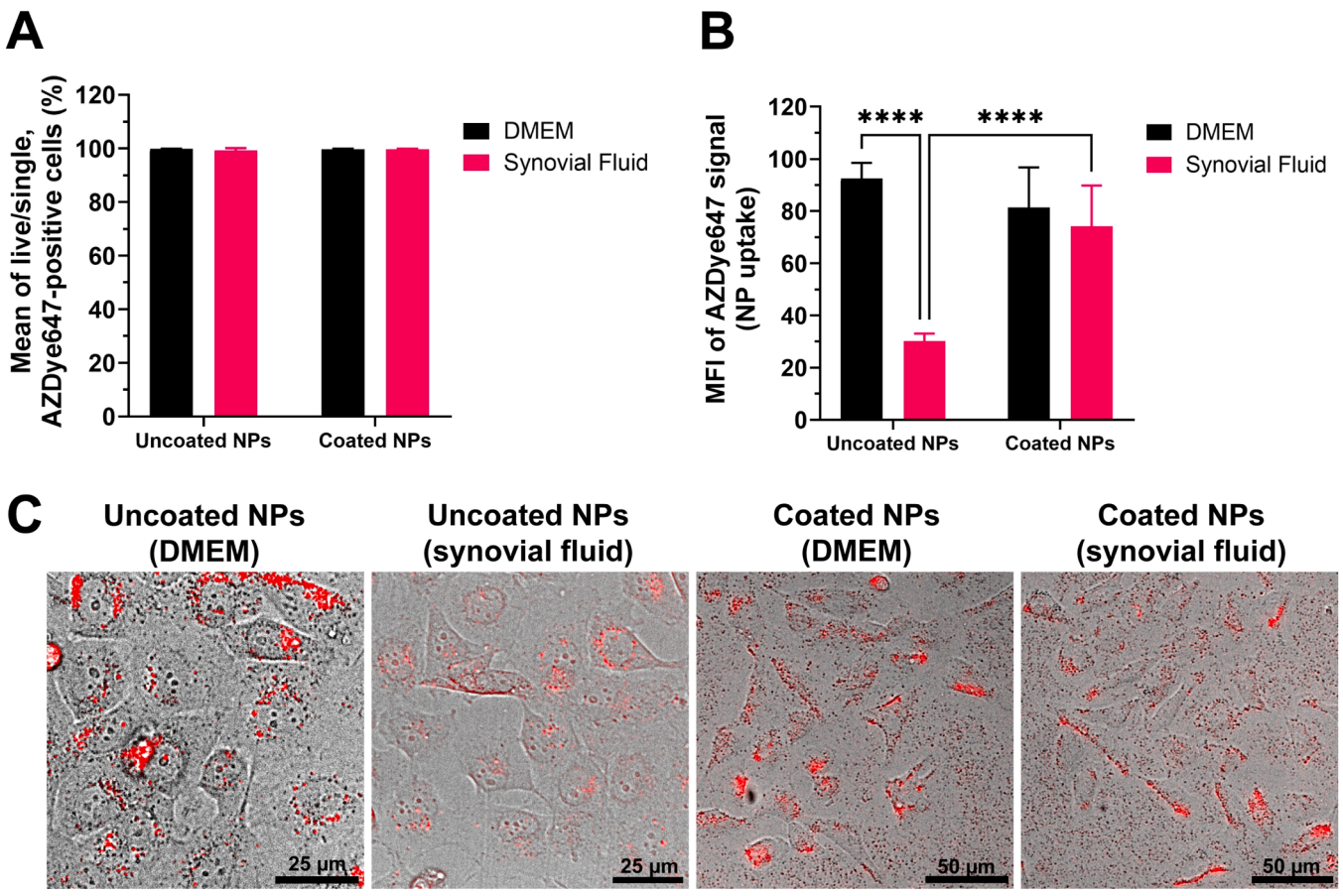

Fig. 2. Uptake of ps-PAAQ NPs after transfection in C28/I2 chondrocytes. **(A)** The percentage of AZDye647-positive cells was determined by FACS after 24 h by the gating of live, single cell events. **(B)** The median fluorescence intensity (MFI) was calculated from the population of live and single cells. The results are the average of triplicates from 3 independent cultures ($n = 3$, Two-Way ANOVA followed by Tukey's test). Statistically significant difference is indicated by (****) to p-value ≤ 0.0001. **(C)** Overlay of bright field and fluorescent images showing NP uptake (red color).

internalized ps-PAAQ NPs. The main difference was found in the MFI of the cells transfected with the uncoated NPs in the presence of synovial fluid, which showed 3-fold lower fluorescence compared with transfection with uncoated NPs in DMEM (Fig. 2B, C). Interestingly, no significant difference in MFI was observed for coated NPs in transfections with either DMEM or synovial fluid (Fig. 2B, C). Besides, the coated NPs in synovial fluid showed significantly higher MFI than the uncoated NPs in synovial fluid. These results suggest that, in the presence of synovial fluid, PEG-coated NPs are better internalized by C28/I2 cells than uncoated NPs, and virtually with the same efficiency as in DMEM only.

In parallel to NP uptake, we also analyzed the GFP expression in C28/I2 cells transfected with ps-PAAQ NPs in DMEM or in 10 % v/v synovial fluid (% of GFP-positive cells). Fig. 3A shows that transfection efficiency was very high for all conditions (≥80 %). Non-transfected cells are shown in **Supplementary Fig. S3**, with no visible green fluorescent signal. Even though statistically significantly lower for the uncoated NPs in DMEM (80 % ± 9 %), the percentage of GFP-positive cells for this condition was still very close to the average transfection efficiency of the other groups (≈90 %). In contrast, the MFI of uncoated NPs in DMEM was significantly higher than PEG-coated NPs (Fig. 3B). Similarly to the uptake, the main difference was found in the MFI of the uncoated NPs that were transfected in the presence of synovial fluid, which resulted in 3.5-fold lower fluorescence compared with uncoated NPs in DMEM (Fig. 3B, C). Also, in line with the effects on uptake, no significant difference in MFI was observed for coated NPs in transfections with either DMEM or synovial fluid (Fig. 3B, C). Despite the significantly higher uptake MFI in synovial fluid using the coated NPs compared to non-coated (Fig. 2B), the MFI of the GFP signal in cells was not statistically higher (Fig. 3B). GFP expression levels were notably less affected by the presence of synovial fluid during transfections of the PEG-coated NPs compared with uncoated NPs.

3.3. In a cartilage-on-chip model, uncoated NPs yield higher transfection efficiency than PEG-coated NPs in chondrocytes, but lower efficiency in the presence of synovial fluid

To provide a more biologically relevant simulation of the 3D dynamic microenvironment for nanoparticle diffusion and cellular uptake, we further tested the ps-PAAQ NPs in a cartilage-on-chip model. This platform comprised C28/I2 chondrocytes embedded in a collagen-based hydrogel matrix. The chamber assigned for the cell laden-hydrogel construct is flanked on both sides by perfusion channels to support the delivery of nutrients and nanoparticles. The central chamber is separated from the perfusion channels by an array of pillars to restrict the cell-hydrogel construct to the central chamber matrix (Fig. 4A), without compromising the inwards diffusion of soluble compounds. The uncoated and PEG-coated NPs were loaded with a mixture of labeled (AZDye568) and non-labeled EGFP mRNA, and then diluted in DMEM or synovial fluid before perfusing them in these devices to visualize NP uptake and GFP expression. The size and zeta potential of these formulations were the same as the formulations prepared for the 2D chondrocyte culture (data not shown). First, we evaluated the diffusion of both NP types for 2 h through the 3D-collagen matrix without cells. The PEG-coated NPs showed a higher and sustained fluorescent signal over time, up to a distance of 0.60 mm in the hydrogel (**Supplementary Fig. S4**). Both uncoated and PEG-coated NPs showed the highest

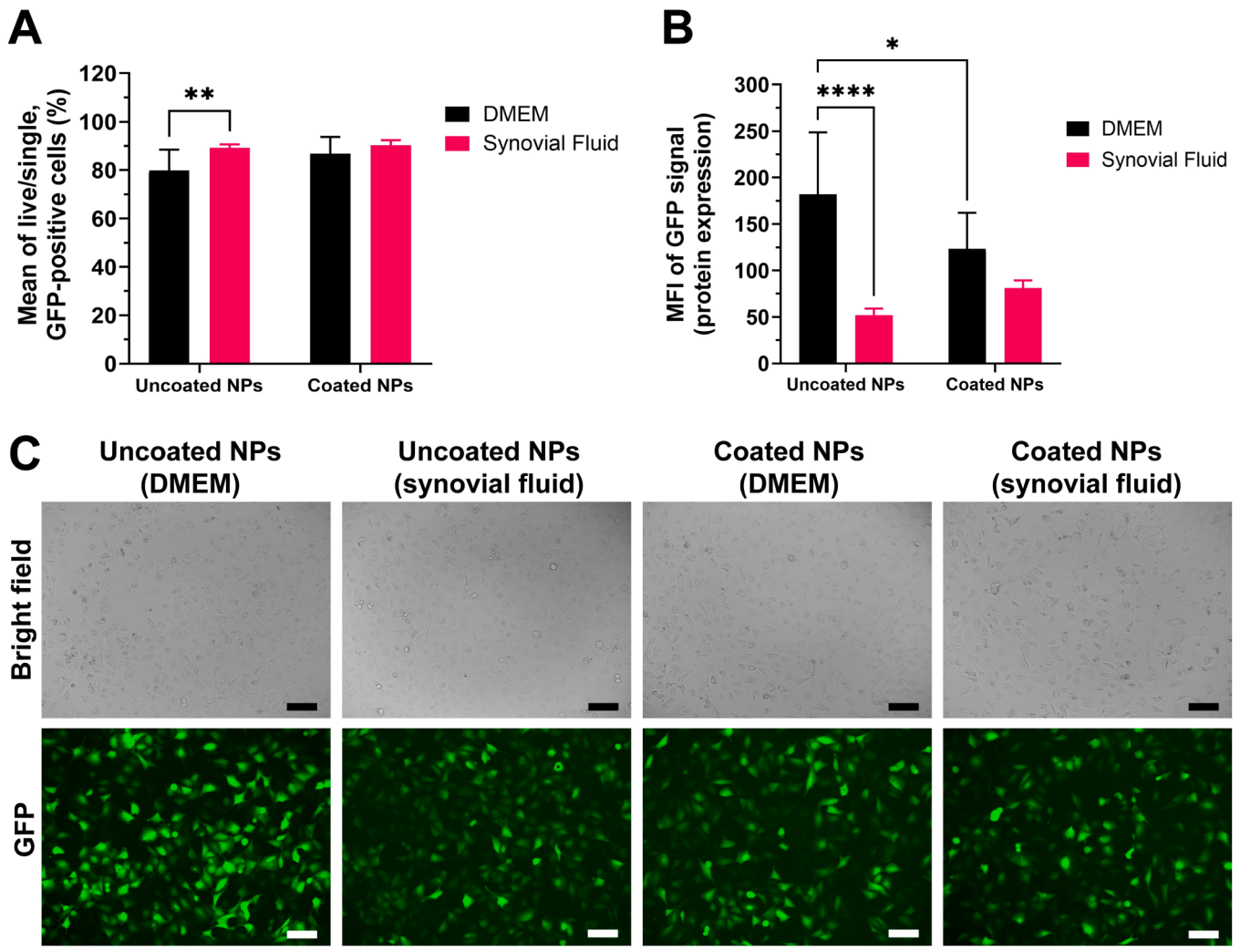

Fig. 3. GFP expression after transfection of C28/I2 chondrocytes with ps-PAAQ NPs. **(A)** The percentage of GFP-positive cells was determined by FACS after 24 h by the gating of live, single cell events. **(B)** The median fluorescence intensity (MFI) was calculated from the double-positive gate (AZDye647+ and GFP+) to include only transfected, live and single cell events. The results are the average of triplicates from 3 independent cultures ($n = 3$, Two-Way ANOVA followed by Tukey's test). Statistically significant difference is indicated by (*) to p-value ≤0.05, (**) to p-value ≤0.01, or (****) to p-value ≤0.0001. **(C)** Bright field and GFP fluorescence images showing the different conditions. Scale bar: 100 μm.

accumulation in the first 0.10 mm of the hydrogel over time, but uncoated NPs tended to not diffuse further than 0.30 mm.

Cell viability in cell containing chips was performed by the fluorescent-based Live/Dead assay. After 24 h of transfection, both uncoated and PEG-coated NPs were well tolerated by C28/I2 cells with a viability >92 % in all conditions (**Supplementary Fig. S5**). In another experiment, transfection efficiency was analyzed after 24 h as the percentage of GFP-positive cells (Fig. 4). It should be noted that Hoechst fluorescence intensity may vary depending on the diffusion of the dye through the hydrogel, but GFP intensity is consistent in all images. Uncoated NPs in DMEM showed the highest proportion of GFP-expressing cells in this experiment (≈18 %), being 2.5-fold higher than their coated counterparts in the same medium (Fig. 4B, C). The nanoparticle diffusion into the matrix and the cellular uptake were also clearly visible, as observed by the bright red spots throughout the hydrogel and around the nuclei of chondrocytes (Fig. 4C, D). When nanoparticles were diluted in synovial fluid before injecting them into the devices, a significant decrease in the percentage of GFP-positive cells was observed for uncoated NPs (Fig. 4B, D). In contrast, with PEG-coated NPs no significant difference in GFP expression between DMEM and synovial fluid was shown. Therefore, these results are in line with the MFI outcomes from the 2D chondrocyte culture in Fig. 3B.

3.4. NPs show uptake in the cartilage of mouse knee joints cultured ex vivo

In order to determine the penetration and cell uptake of ps-PAAQ NPs in cartilaginous tissue, we applied an *ex vivo* model consisting of mice knee joints for visualization of NP localization by confocal microscopy. The uncoated and PEG-coated NPs were loaded with a mixture of labeled (AZDye568) and non-labeled EGFP mRNA, and the cartilage uptake/penetration was examined. As a negative control, we used PEG-coated ps-PAAQ NPs loaded only with luciferase mRNA ("non-fluorescent NPs"). These NPs showed similar particle size properties (54.1 nm; PDI 0.078 ± 0.016) and zeta potential (−1.6 ± 0.7 mV) as their fluorescent counterparts. The particle size distribution is shown in **Supplementary Fig. S6**.

Decalcified mouse knee joints were frozen, sectioned and analyzed by fluorescence microscopy. The fluorescent signal from the ps-PAAQ NPs localized in the cartilage was found in images from two out of four injected joints per group (Fig. 5). The perinuclear localization of the fluorescent signal suggests that the NPs were endocytosed by chondrocytes. Penetration to the calcified layers of the cartilage was not observed, as the fluorescence levels were similar to the background fluorescence from the negative control (Fig. 5A). No fluorescent signal

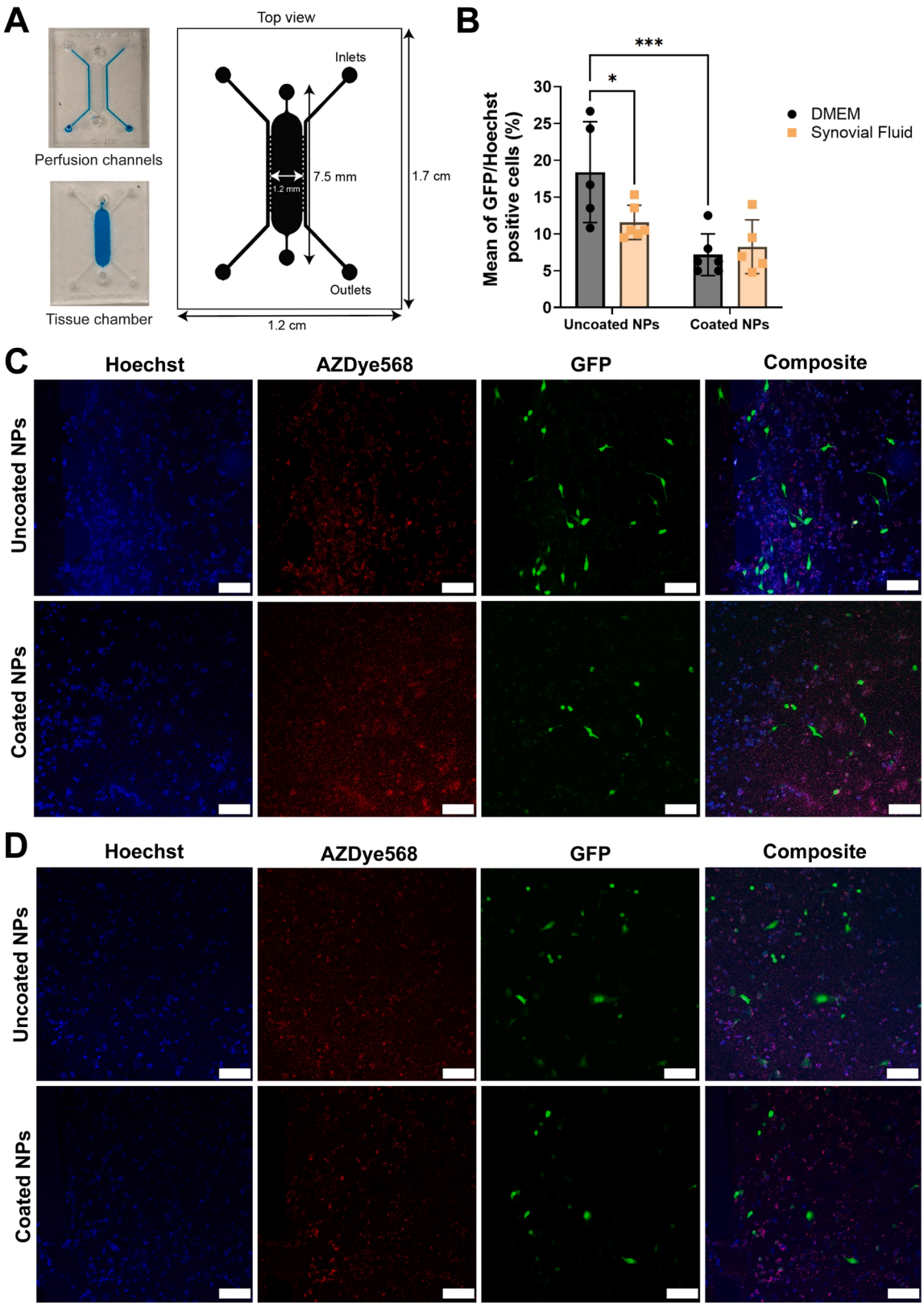

Fig. 4. Cartilage-on-chip platform showing uptake of ps-PAAQ NPs and GFP expression in C28/I2 chondrocytes. **(A)** Design and top view of the cartilage-on-chip, highlighting its main features and dimensions. The device was injected with a dye for visualization of the perfusion channels and central tissue chamber. **(B)** Transfection efficiency as expressed by the percentage of GFP-positive cells (Two-Way ANOVA followed by Fisher's LSD test). Statistically significant difference is indicated by (*) to p-value $\leq$0.05, or (***) to p-value $\leq$0.001. **(C)** Uptake and GFP expression for ps-PAAQ NPs diluted in DMEM. **(D)** Uptake and GFP expression for ps-PAAQ NPs diluted in 10 % v/v synovial fluid. First column shows nuclear staining with Hoechst; second column shows NP diffusion/uptake (AZDye568-labeled mRNA); third column shows GFP-expressing cells; last column displays the overlay of all channels. Scale bar: 100 μm.

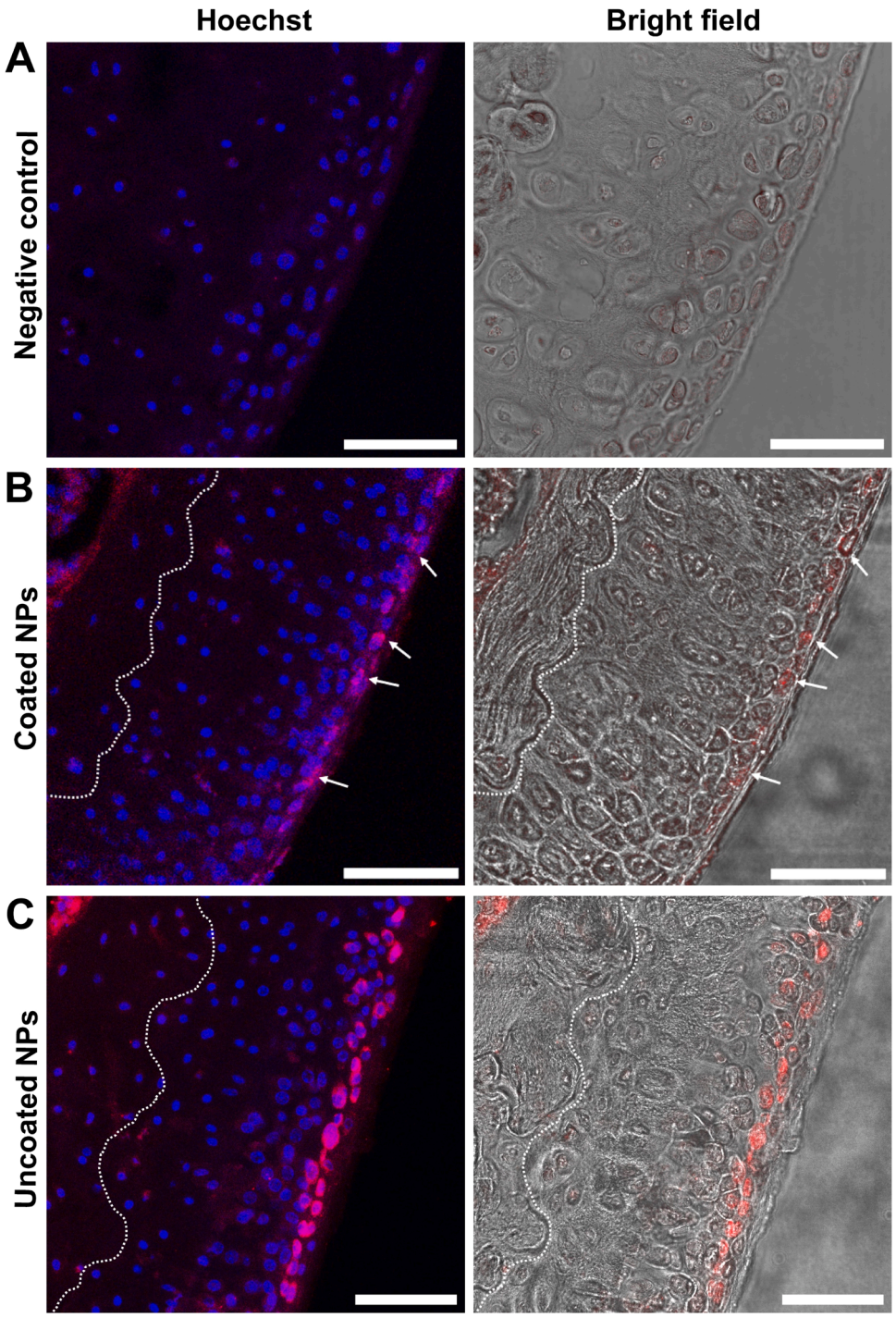

Fig. 5. Uptake of ps-PAAQ NPs in the articular cartilage of mouse knee joints cultured *ex vivo*. **(A)** Negative control: knee joints injected with ps-PAAQ NPs loaded with non-labeled mRNA ("non-fluorescent NPs"). **(B, C)** Knee joints injected with PEG-coated or uncoated ps-PAAQ NPs showing uptake in cells of the superficial layer of the cartilage. Fluorescent NPs were loaded with AZDye568-labeled mRNA (red color). First column shows the overlay of NPs with Hoechst 33342 used for nuclear staining; second column shows the overlay of NPs with bright field. Dotted line represents the limit between the subchondral bone and the articular cartilage. Scale bar: 50 μm.

was found in the synovial lining. The more fibrous joint structures such as ligaments and menisci showed very high auto-fluorescence making it difficult to distinguish the NPs. Although visualization of nanoparticle uptake in the cartilage was possible, we could not detect GFP expression. Overall, these results suggest that ps-PAAQ NPs can be taken up efficiently by chondrocytes in the superficial layer of the cartilage of mouse knee joints, which is a native tissue rich in extracellular matrix.

3.5. Intra-articular administration of ps-PAAQ NPs in rats does not promote cartilage damage, but induces synovial inflammation

As a preliminary safety check for *in vivo* injection of luciferase mRNA-loaded ps-PAAQ NPs, we qualitatively assessed whether it promoted any damage to the cartilage or inflammation in the synovium (synovitis). For this, tissue sections of the cartilage and synovial lining were obtained from rat knee joints (healthy and OA-induced), 28 days

after the first IA injection and euthanasia. Any cartilage damage was scored using the Mankin histological-histochemical grading method. The scores of the medial and lateral tibial plateau and medial and lateral femoral condyle (**Supplementary Fig. S7**) were combined, resulting in a total Mankin score per rat knee joint (Fig. 6). Fig. 6A appears to show no difference between uncoated and PEG-coated NPs, suggesting that the NP type did not influence the OA progression at the cartilage level. The OA-inducing surgery resulted in a visible difference in total Mankin scores between all averaged healthy and osteoarthritic knees (Fig. 6A). Importantly, the NP injection did not induce cartilage damage when injected into healthy knee joints, although signs of synovitis were observed (Krenn score).

The histological changes in the cartilage can be observed in Fig. 6C, where the medial tibial plateau and femoral condyle are compared to each other, for both healthy and osteoarthritic knee joints injected with NPs. Compared to healthy joints, we observed a considerable decrease in Safranin-O staining in osteoarthritic joints, revealing the reduction in the proteoglycan content and indicating cartilage degeneration. Additionally, surface irregularities can be observed throughout the surface of the osteoarthritic joints, as well as a visible decrease in the number of tissue-resident chondrocytes (Fig. 6C).

Synovial inflammation was scored using the histopathological Krenn score. While no visible difference was found between uncoated and PEG-coated NPs, all joints displayed low-to-high grade synovitis following NP injection, with an increasing trend in OA knee joints (Fig. 6B). This indicates that the IA injection of ps-PAAQ NPs (10 μg mRNA dose) promotes synovial inflammation in rat knee joints, even though in the healthy joints no cartilage damage was detected. The changes in the synovial membrane can also be observed in Fig. 6D, which depicts the hallmarks of synovitis including lining layer hyperplasia, activation of resident stromal cells and the presence inflammatory infiltrates. These findings are observed in both healthy and OA-induced knee joints injected with NPs, being more pronounced in the osteoarthritic joints.

3.6. In vivo administration of ps-PAAQ NPs in rats is efficient for local mRNA delivery and luciferase expression

Twenty-eight days after inducing OA surgery (day 0), the rats received IA injections with luciferase mRNA-loaded ps-PAAQ NPs (Table 1). One week later (day 7), a second injection was performed using the same dosage. Both uncoated and PEG-coated NPs were successfully delivered to the knee joints, as shown by the presence of the near-infrared (NIR) dye bound to luciferase mRNA for 28 days (Fig. 7). For all the mRNA concentrations, a higher peak of NIR signal was observed immediately after injection, on days 1 and 8, respectively (Fig. 7A, **Supplementary Fig. S8**). Then the NIR signal decreased in the following days, but did not disappear completely by the end of the experiment. For the highest mRNA dose (10 μg mRNA), the uncoated NPs injected in healthy knees showed a more consistent delivery and retention throughout the experiment. This effect was particularly evident after the second injection, with a statistically higher NIR signal compared with at least one of the other groups on days 1, 8, 10, 12, 21 and 28 (Fig. 7A). This can be observed in Fig. 7B, which depicts the NIR signal in both knees from a rat injected with uncoated NPs (10 μg mRNA), showing consistently a higher NIR signal in the healthy knees than OA knees over time. This difference was not observed at lower mRNA doses (**Supplementary Fig. S8**), which showed either no statistical differences between groups (7.5 μg mRNA dose), or instead showed significantly higher NIR signal for uncoated NPs injected in OA knees on days 7, 12 and 14 (5 μg mRNA dose).

The mRNA encoding for luciferase was translated in the rat knee joints one day after the first IA injection of both uncoated and PEG-coated NPs, as shown by bioluminescence imaging (BLI) (Fig. 8A). Because of loss of signal over time, BLI was only performed on days 1, 3 and 8. Fig. 8B shows the bioluminescence for the highest mRNA dose (10 μg mRNA) delivered by uncoated and PEG-coated NPs. However, no protein expression was detected 3 days after the first mRNA injection, nor was a bioluminescent signal observed after the second injection (day 8). As shown in Fig. 8A, no signal could be detected in healthy knees after luciferase mRNA delivery by uncoated NPs at any concentration, suggesting that mRNA was not translated. For the higher mRNA doses (7.5 and 10 μg mRNA), a significantly higher signal was visible in OA knees injected with uncoated NPs compared with healthy knees. These findings contrast with results from Fig. 7A, which shows on day 1 significantly higher local delivery of uncoated NPs in healthy knees compared with OA knees. Interestingly, luciferase mRNA delivery by PEG-coated NPs resulted in a detectable bioluminescent signal in both healthy and diseased knees at all concentrations (Fig. 8A), with a linear dose-dependent effect ($R^2 = 0.96$ for healthy knees and $R^2 = 0.83$ for OA knees). Regarding the injected mRNA dose only (main effect), a significant difference was observed between the 5 μg mRNA and 10 μg mRNA doses ($p = 0.0168$).

4. Discussion

In this study, we showed that ps-PAAQ NPs are a promising carrier for intra-articular delivery of mRNA for therapeutic applications in osteoarthritis. By comparing two variants of this delivery system – uncoated and PEG-coated NPs – we applied a range of models to evaluate local mRNA delivery and protein expression. In the presence of synovial fluid, PEG-coated NPs resulted in higher endocytosis than uncoated NPs in 2D culture, and equivalent GFP expression as uncoated NPs in the 2D culture and cartilage-on-chip (also with synovial fluid). *In vivo,* uncoated NPs showed higher retention in healthy knee joints compared to PEG-coated NPs, whereas for the two higher concentrations of uncoated NPs (7.5 and 10 μg mRNA) expression was higher in OA joints compared to healthy joints. This difference in disease status was not noted for PEG-coated NPs, as these showed more consistency in terms of luciferase expression in healthy and OA knees.

The interactions with synovial fluid are a determinant for NP fate in the joint, inducing changes to the hydrodynamic diameter and surface properties of particles that can affect NP distribution and stability. The (cationic) uncoated NPs were more affected by incubation with synovial fluid, displaying higher hydrodynamic diameter (>700 nm) and a shift in zeta potential (from strongly positive to neutral values). The effect of charge reversal seems to be particularly impacting for cationic polymers, as previously reported for dimethylamine borane (DMAB) NPs, which underwent a notable shift in surface charge upon incubation with bovine synovial fluid (from +24.6 mV to −10.9 mV) [22]. The synovial fluid contains high levels of plasma proteins, mainly anionic albumin and hydrophobic globulins, and hyaluronic acid. Hyaluronic acid is an anionic, nonsulfated glycosaminoglycan that could interact with amine groups of the ps-PAAQ polymer and change the surface charge of the NPs to neutral. NPs with a neutral surface show increased reversible aggregation resulting in larger particle size measurement. These changes in physicochemical properties may also be explained by the formation of a protein corona that affects colloidal stability and leads to particle aggregation [31]. In our experiments, the PEG-coated NPs were virtually unaffected by the components of the synovial fluid, keeping their small size (≈50 nm) and neutral zeta potential (≈0 mV) unchanged as in the original formulation buffer (10 mM histidine 10 % trehalose). This can be explained by the addition of the hydrophilic $PGA_{7.5k}$-PEG_{5k} coating, which shields the NP surface from interaction with components of the synovial fluid, thereby potentially preventing particle aggregation and a shift in zeta values. This shielding effect provided by our coating contrasts with the changes observed in a similar study [21], in which PAMAM dendrimers were modified with $mPEG_{5k}$ and incubated with synovial fluid from OA patients, showing increased NP sizes and a shift toward negative charges (from +4.0 to −13.9 mV). These changes were owing to protein adsorption to NP surfaces, as measured by protein quantification of adhered proteins from OA SF-derived coronas.

In the 2D chondrocyte culture, cellular internalization of uncoated

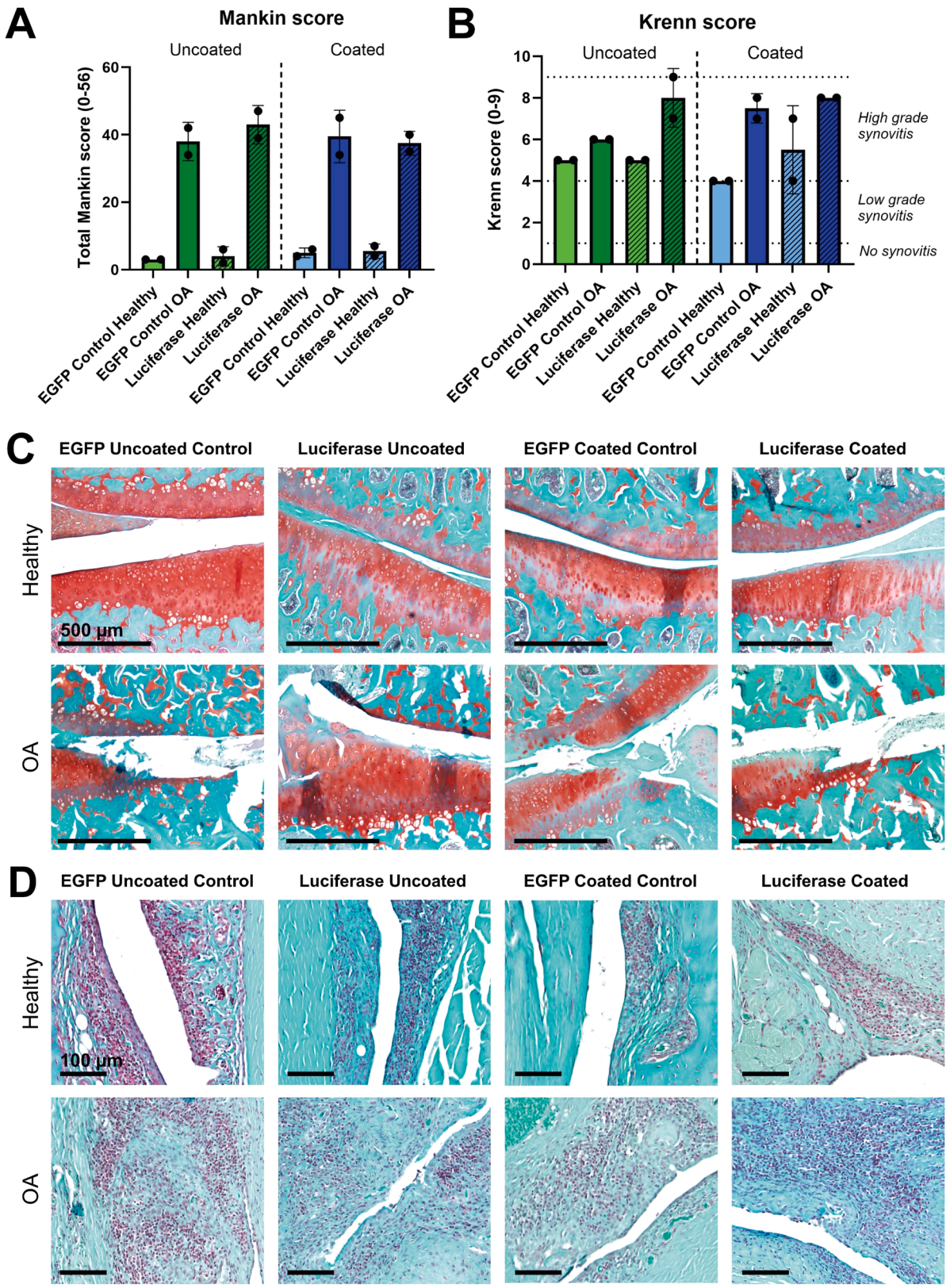

Fig. 6. Histological-histochemical scoring of healthy and OA rat knee joints injected with ps-PAAQ NPs. NPs were loaded with luciferase mRNA or EGFP mRNA (control group). **(A)** Total Mankin scores for cartilage damage. **(B)** Krenn scores for synovial inflammation. **(C)** Safranin-O/Fast-Green/Hematoxylin staining of healthy and osteoarthritic cartilage from medial femorotibial joints. **D.** Hematoxylin & Eosin staining of healthy and osteoarthritic synovial lining from femorotibial joints. Safranin-O stains proteoglycans in red, Fast-Green stains non-collagen tissue components in green, Hematoxylin stains cell nuclei in dark-purple and Eosin stains the cytoplasm/extracellular matrix in pink.

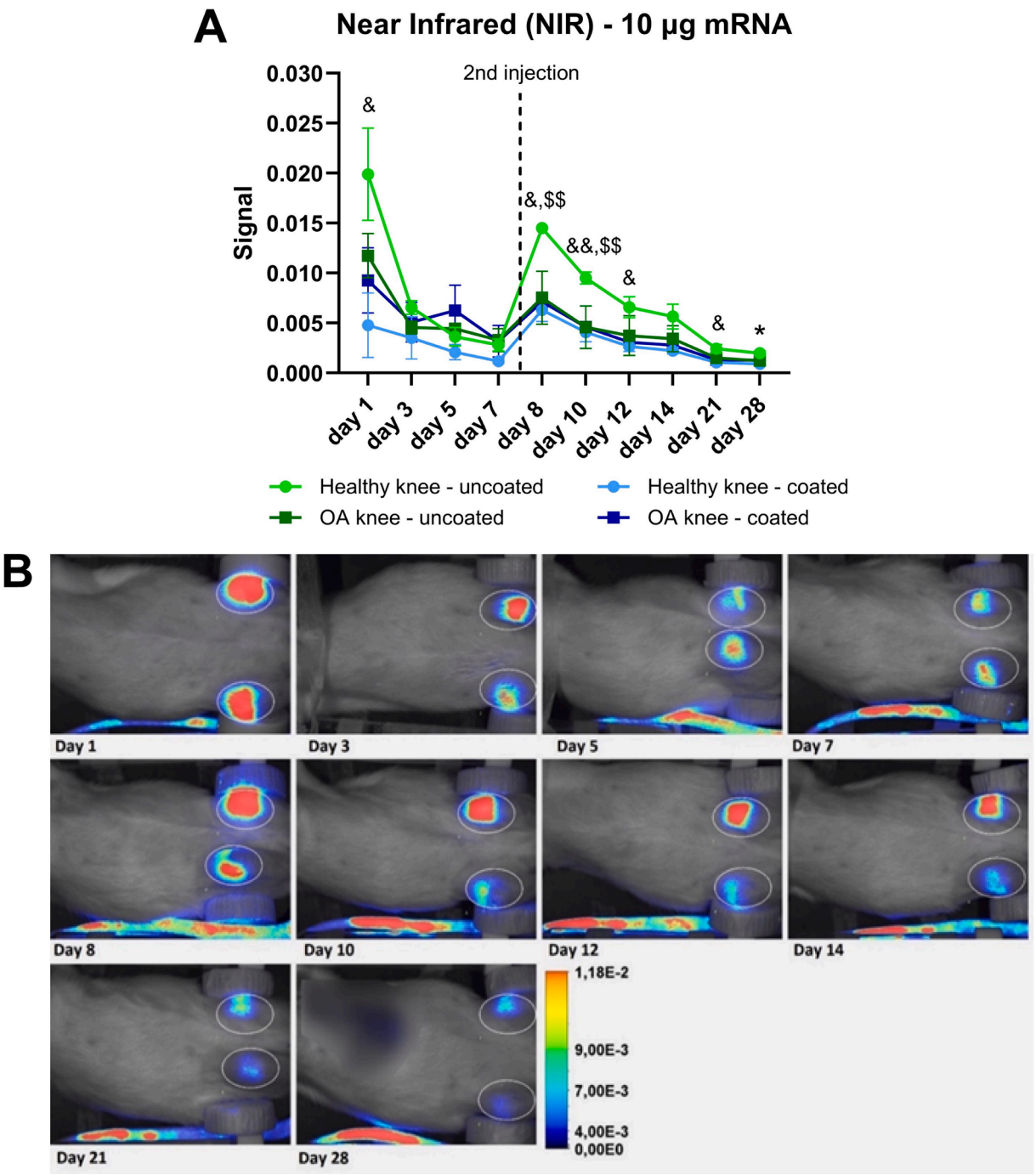

Fig. 7. NIR signal in healthy and OA-induced rat knees after intra-articular injection of ps-PAAQ NPs. **(A)** Results with the 10 µg mRNA concentration. Injections were performed on day 0 and day 7 (dotted line on the graph). The results are the average from 3 animals per group ($n = 3$, linear mixed model followed by Tukey's test). Statistical significance (p-value ≤ 0.05) is indicated by (&) for difference between "Healthy knee – uncoated" *vs.* "Healthy knee – coated", ($) for difference between "Healthy knee – uncoated" *vs.* "OA knee – coated", or (*) for difference between "Healthy knee – uncoated" *vs.* all other groups. The duplicate of any of these symbols represents a p-value ≤ 0.01. **(B)** Representative NIR images of a rat from group "10 µg mRNA uncoated" throughout the experiment. The left knee (upper knee) is healthy, and the right knee (lower knee) is osteoarthritic.

NPs was significantly lower in the presence of synovial fluid compared with transfections in DMEM only, as was the subsequent GFP protein expression (MFI signal). This may be explained by the significant modification of the NP properties after dilution in synovial fluid, potentially affecting the NP interactions with the target cell membrane. This is relevant to the biological efficacy, as the interplay between different particle sizes and surfaces charges may change the endocytic pathway of the NPs [32]. On the other hand, transfections with PEG-coated NPs in synovial fluid showed no significant effect of SF on cell uptake and GFP expression. These coated nanoparticles also displayed remarkably higher uptake by cells in the presence of synovial fluid than their uncoated counterparts, even though GFP expression was not significantly different, which may suggest a different endocytic mechanism for PEG-coated NPs leading to lower translation efficiencies. The results from 2D culture were further corroborated by our cartilage-on-chip model containing a 3D-collagen matrix, in which the percentage of GFP-positive chondrocytes was significantly reduced by the presence of synovial fluid during the transfection with uncoated NPs.

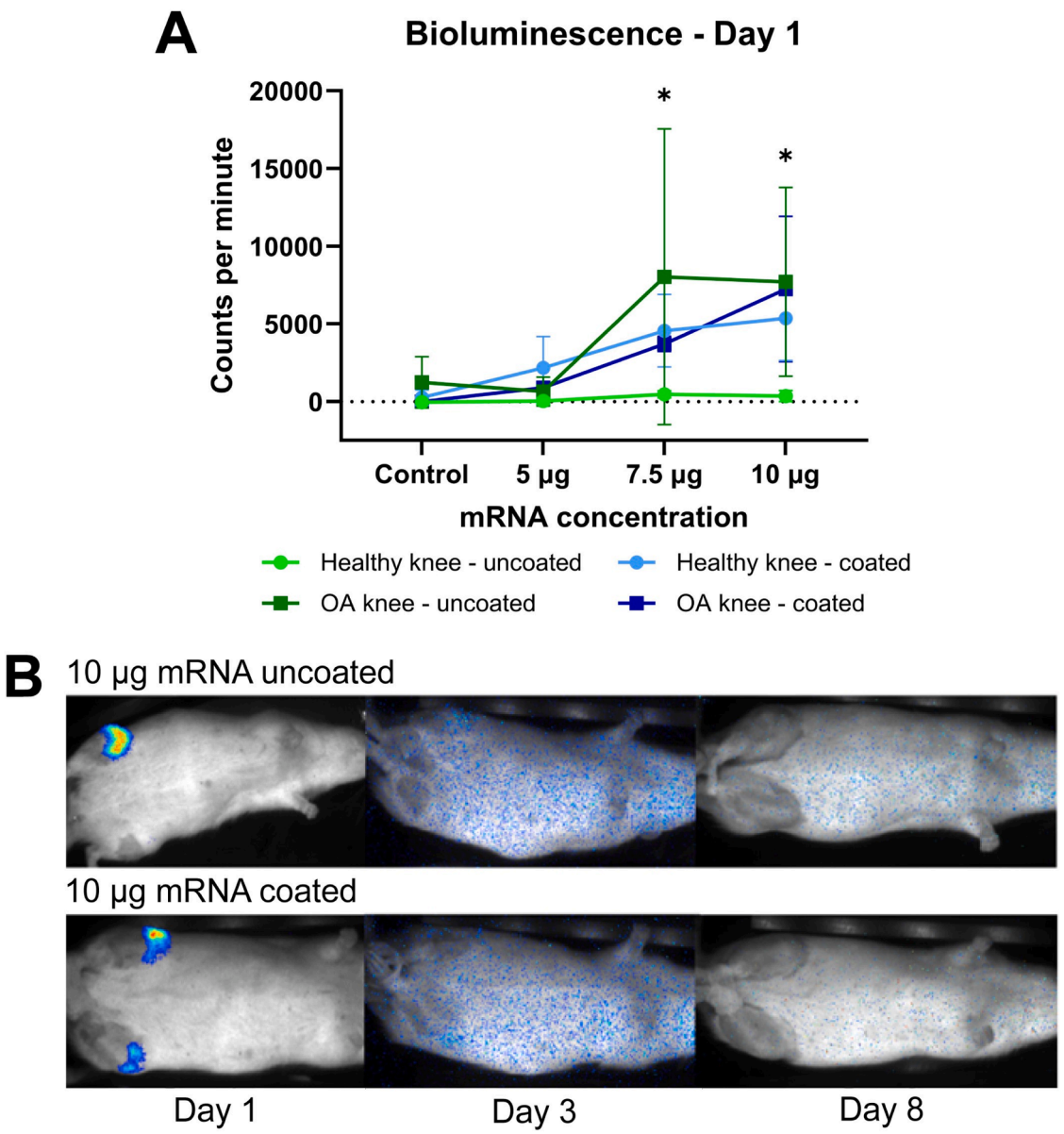

Fig. 8. Bioluminescence imaging (BLI) in healthy and OA-induced rat knees after intra-articular injection of ps-PAAQ NPs. **(A)** Bioluminescence on day 1 after first injection, for all experimental groups and mRNA concentrations. BLI is expressed as the photon counts per minute. The results are the average from 3 animals per group ($n = 3$, Two-Way ANOVA followed by Tukey's test). Statistical significance (p-value ≤ 0.05) is indicated by (*) for difference between "Healthy knee – uncoated" *vs.* "OA knee – uncoated". The control group consists of uncoated and PEG-coated NPs loaded with EGFP mRNA, injected into the knees at a 10 µg mRNA dose. **(B)** Representative images of a rat from groups "10 µg mRNA uncoated" and "10 µg mRNA coated", after BLI on days 1, 3, and 8. Injections were performed on day 0 and day 7. The right knee (upper knee) is healthy, and the left knee (lower knee) is osteoarthritic.

This reduction was not observed for PEG-coated NPs, and both NP types showed equivalent GFP expression in synovial fluid, also in line with the MFI results from 2D culture. In general, a lower transfection efficiency was found in this cartilage-on-chip model, most likely due to the presence of a dense collagen matrix. PEG-coated NPs showed better penetration through this 3D microenvironment than uncoated NPs, probably because of their reduced particle size and monodispersity. Although the chip model does not fully recapitulate the native joint environment, it could clearly simulate a protein-rich environment that influences NP migration and biological function. Altogether, these results suggest that, even though uncoated NPs achieved higher GFP expression in DMEM, the PEG-coated NPs showed favorable properties for better penetration. These studies highlighted the impact of synovial fluid and NP properties on cell transfection.

The *ex vivo* short-term NP exposure in mouse knee joints, following IA injection, suggested that uncoated and PEG-coated ps-PAAQ NPs showed visible uptake by chondrocytes in the superficial zone of the cartilage. In both cases, penetration to the calcified layers of the cartilage did not seem to occur. While in some situations full penetration into cartilage is desired, superficial zone accumulation and subsequent protein expression *in vivo* can still lead to therapeutic efficacy. As the superficial zone is where OA degeneration begins, it may be sufficient to deliver mRNA immediately to this location. Why the uptake of uncoated NPs was reduced in the presence of synovial fluid compared with PEG-coated NPs in our *in vitro* studies, whereas both appeared to be taken up in the *ex vivo* model is unclear. The negative charges from glycosaminoglycan (GAG) chains of proteoglycans in the cartilage matrix may make the cationic NPs preferrable for OA treatment, by providing favorable electrostatic interactions for passive targeting of chondrocytes. Nanoparticles that demonstrate stronger biophysical

interactions with the cell membrane also tend to show greater cellular uptake [33]. Cationic NPs usually exhibit greater cell uptake due to increased electrostatic interactions with negatively charged cell membranes (*i.e.*, membrane distortions or "holes" formation), whereas anionic and neutral NPs are internalized into cells only *via* endocytic pathways [34,35]. Besides, different proteins from the synovial fluid may adsorb onto uncoated and PEG-coated NP surfaces, and the specific makeup of the protein corona might be correlated with enhanced cell association and uptake of a given NP type as shown in other studies [21, 36]. Considering that the uptake of ps-PAAQ NPs by the cartilage occurs essentially by diffusion in this *ex vivo* model (no biomechanical stimulation), possibly charge interactions between cationic NPs and the anionic ECM may play a more important role in mRNA delivery than the nanoparticle size alone in this model. However, as the number of animals used was limited and uptake highly variable associated with the challenges of mouse joint injection, it is not possible to draw definite conclusions from this study.

In vivo, the ps-PAAQ NPs were efficient for local delivery of mRNA in healthy and OA knee joints of rats, showing retention up to 4 weeks after the first IA injection. Interestingly, uncoated NPs showed a significantly higher localization in the healthy knee joints at all timepoints (10 μg mRNA dose). However, the detection of labeled mRNA was not correlated with luciferase expression, as the latter was detectable only 24 h after first injection. In a previous study [12], intra-articular delivery of PEG-polyamino acid nanomicelles carrying 1 μg luciferase mRNA induced signal in intact mouse knee joints at 24 and 48 h after injection, but then this signal rapidly decreased and reached an undetected level at 4 days after injection. Even though this may not be directly translated to our rat model (different species), it could be an indication that the maximum concentration of 10 μg mRNA used in this study is not enough to sustain luciferase expression. Also, the fluorescently labeled mRNA may not correspond to luciferase mRNA that is still intact and available for translation. In addition, the complete absence of expression upon a second injection of mRNA-loaded NPs, suggests an immune response, innate or acquired. The increased synovitis suggested in the safety study may support this explanation. Scavenging of NPs by an increased presence of macrophages may play a role here, as we showed previously that M1-like macrophages in 2D culture efficiently internalized ps-PAAQ NPs but did not express the delivered mRNA [37]. The discord between the presence of labeled mRNA and final protein expression was also evident in the joints injected with uncoated NPs. Despite higher mRNA retention in healthy joints compared to OA joints, luciferase expression was only detectable in OA knee joints using uncoated NPs. In contrast, PEG-coated NPs induced luciferase expression in a dose-dependent fashion independent of disease status. These results were unexpected, and we can speculate two hypotheses for them. Firstly, the more consistent expression observed for PEG-coated NPs may be a consequence of their better stability profile than uncoated NPs, as we previously demonstrated by mRNA integrity in agarose gel [23]. Secondly, these findings might be related to the architectural changes of the cartilage tissue in the course of OA progression. The accompanying depletion of proteoglycans and collagen in the ECM may increase the tissue pore size, allowing better diffusion of nanoparticles than normal cartilage [38]. Moreover, in OA the composition of the synovial fluid also changes, with a reduction of the molecular weight and concentration of hyaluronic acid, thereby lowering fluid viscosity and elasticity [39]. This may also favor the colloidal stability and diffusiveness of NPs before they reach into the cartilage. Given the higher particle size of uncoated NPs and their aggregation in synovial fluid, it may be possible that these NPs showed lower lymphatic clearance but were unable to penetrate the healthy cartilage from rats and deliver the mRNA into chondrocytes, while the smaller and uniform PEG-coated NPs could transfect them more easily. In the more porous osteoarthritic cartilage (lower size exclusion), the positive charges of uncoated NPs might have turned into an advantage for cartilage penetration and intracellular delivery as alluded to in the *ex vivo* model, by providing electrostatic interactions with negatively charged components of the ECM and cell membranes, thus resulting in higher luciferase expression.

The results of the *in vivo* experiments should be interpreted with caution given the small sample size per group ($n = 2$ for histological scoring; $n = 3$ for NIR/BLI studies), and the variability in the data at higher mRNA doses. However, it should be noted that no irregularities were reported during injections and that these studies were more focused on general aspects (*e.g.*, interactions between NP type and disease state), rather than detecting statistically significant differences between specific mRNA concentrations or timepoints. On a different note, further investigation into the exact tissue/cell type transfected by ps-PAAQ NPs is needed, as the *in vivo* imaging provided the signal in whole joints. Consequently, it was not possible to know whether the luciferase signal was coming directly from the cartilage, synovial lining, or the surrounding tissues within the joint (*e.g.*, ligaments, menisci, tendons). Regarding the limitations of the *ex vivo* model applied in this study, we could not detect GFP protein expression in the cartilage. Since we were using knee joints of mouse cadavers in this model, we could not ensure full viability of the chondrocytes in the cartilage. Another reason might be the GFP protein denaturation due to the processing of knee joints (fixation/decalcification), leading to loss of signal. Other general constraints of this model are the absence of biomechanical stimulation (*i.e.*, static culture) and the thin anatomy of the mouse articular cartilage (≈50 μm compared to 1.5–2.0 mm in humans [40]). The small dimensions of the mouse joint cavity also curb the tolerated volumes of NPs for injection (<6 μL), in order to prevent leakage and joint swelling. Finally, although cartilage integrity was not affected by the injections, the low-to-high grade synovial inflammation found in all conditions (healthy/OA knee joints) in the rat study deserves further research. It is known that intra-articular injection is frequently associated with transient increases in pain and/or inflammation, even with substances such as hyaluronic acid [41]. Further investigation is needed to verify whether this is caused by an immune response against the NPs or the mRNA payload, and to what extent this affects the disease in the long term.

5. Conclusion

In summary, we demonstrated for the first time the application of ps-PAAQ NPs as nanocarriers for intra-articular delivery of mRNA in knee joints. The range of models used in this study – 2D chondrocyte culture in the presence of synovial fluid, cartilage-on-chip-platform, *ex vivo* culture of mouse knee joints, and *in vivo* OA rat model – provided a protein-rich microenvironment that is designed to be challenging for mRNA delivery. At the same time, they also showed how crucial it is to validate novel delivery systems in models mimicking the joint milieu (*e.g.*, synovial fluid and a dense ECM), given the contradictory results that may be observed as the biological complexity increases. While the neutral PEG-coated NPs showed more benefits *in vitro* when in contact with synovial fluid, uncoated NPs showed more *in vivo* retention in healthy knee joints of rats over time. However, in terms of *in vivo* luciferase expression, the PEG-coated NPs were less dependent on disease state and worked well both in healthy and OA knee joints. These results suggest that, apart from nanoparticle size, electrostatic interactions between cationic NPs and the anionic components of the ECM play a key role in cartilage penetration and mRNA delivery to tissue-resident chondrocytes. Besides, the interplay between the disease state (healthy/OA knees) and the NP properties also seems to be relevant. Although our findings are promising, further *in vivo* studies using larger OA animal models are needed to bridge the gap to application in clinical practice. Also, considering that synovial inflammation was observed in all groups injected with the mRNA-loaded NPs, further platform and dose optimization are required for a fine tuning between protein expression and biocompatibility. Notwithstanding, this work provides the foundations for future investigations of polymeric nanoparticles for therapeutic mRNA delivery in osteoarthritic joints.

CRediT authorship contribution statement

Adriano P. Pontes: Writing – original draft, Methodology, Formal analysis, Conceptualization, Writing – review & editing, Visualization, Investigation, Data curation. **Jaqueline Lourdes Rios:** Methodology, Formal analysis, Conceptualization, Writing – review & editing, Investigation, Data curation. **Mattie Rijker:** Writing – original draft, Methodology, Formal analysis, Conceptualization, Visualization, Investigation, Data curation. **Kelly Warmink:** Writing – review & editing, Visualization, Formal analysis, Writing – original draft, Investigation, Data curation. **Shreya Gudi:** Writing – review & editing, Visualization, Investigation, Data curation, Writing – original draft, Methodology, Formal analysis, Conceptualization. **Francisco Conceição:** Writing – review & editing, Visualization, Investigation, Writing – original draft, Methodology, Conceptualization. **Björn Meij:** Methodology, Writing – review & editing, Investigation. **Tim J.M. Welting:** Writing – review & editing. **Liliana Moreira Teixeira:** Writing – review & editing, Supervision, Project administration, Conceptualization, Validation, Resources, Funding acquisition. **Jaap Rip:** Validation, Resources, Funding acquisition, Writing – review & editing, Supervision, Project administration, Conceptualization. **Laura B. Creemers:** Writing – review & editing, Supervision, Project administration, Conceptualization, Validation, Resources, Funding acquisition.

Declaration of competing interest

The authors declare the following financial interests/personal relationships which may be considered as potential competing interests:

Authors AP and JR were employed by 20Med Therapeutics BV.

Acknowledgements

The C28/I2 cells used in this study were kindly provided by Prof. Mary B. Goldring (Weill Cornell Medical College, United States). This project has received funding from the European Union's Horizon 2020 research and innovation program under Marie Sklodowska-Curie grant agreement No. 955335 (CARTHAGO) and No. 12792 (JOINT-APPROACH). The luciferase mRNA was kindly provided by Ethris under JOINT-APPROACH. This project has also received funding from the Dutch Research Council (NWO) *perspectief* P20-07.

Supplementary materials

Supplementary material associated with this article can be found, in the online version, at doi:10.1016/j.actbio.2025.06.039.

References

[1] R.F. Loeser, J.A. Collins, B.O. Diekman, Ageing and the pathogenesis of osteoarthritis, Nat. Rev. Rheumatol. 12 (2016) 412–420, https://doi.org/10.1038/nrrheum.2016.65.

[2] D.J. Hunter, S. Bierma-Zeinstra, Osteoarthritis, The Lancet 393 (2019) 1745–1759, https://doi.org/10.1016/S0140-6736(19)30417-9.

[3] J.D. Steinmetz, G.T. Culbreth, L.M. Haile, Q. Rafferty, J. Lo, K.G. Fukutaki, J. A. Cruz, A.E. Smith, S.E. Vollset, P.M. Brooks, et al., Global, regional, and national burden of osteoarthritis, 1990–2020 and projections to 2050: A systematic analysis for the Global Burden of Disease Study 2021, Lancet Rheumatol. 5 (2023) e508–e522, https://doi.org/10.1016/S2665-9913(23)00163-7.

[4] W. Zhang, W.B. Robertson, J. Zhao, W. Chen, J. Xu, Emerging trend in the pharmacotherapy of osteoarthritis, Front. Endocrinol 10 (2019) 431, https://doi.org/10.3389/fendo.2019.00431.

[5] I.A. Jones, R. Togashi, M.L. Wilson, N. Heckmann, C.T. Vangsness, Intra-articular treatment options for knee osteoarthritis, Nat. Rev. Rheumatol. 15 (2019) 77–90, https://doi.org/10.1038/s41584-018-0123-4.

[6] C. Cooper, R. Chapurlat, N. Al-Daghri, G. Herrero-Beaumont, O. Bruyère, F. Rannou, R. Roth, D. Uebelhart, J.-Y. Reginster, Safety of oral non-selective non-steroidal anti-inflammatory drugs in osteoarthritis: what does the literature say? Drugs Aging 36 (2019) 15–24, https://doi.org/10.1007/s40266-019-00660-1.

[7] M.A. Tryfonidou, G. de Vries, W.E. Hennink, L.B. Creemers, Old drugs, new tricks" – Local controlled drug release systems for treatment of degenerative joint disease, Adv. Drug Deliv. Rev. 160 (2020) 170–185, https://doi.org/10.1016/J.ADDR.2020.10.012.

[8] C.H. Evans, V.B. Kraus, L.A. Setton, Progress in intra-articular therapy, Nat. Rev. Rheumatol. 101 (10) (2013) 11–22, https://doi.org/10.1038/nrrheum.2013.159. *2013*.

[9] G.A. Feichtinger, R.M. Raftery, M.B. Goldring, A. Mobasheri, I. Uzieliene, U. Kalvaityte, E. Bernotiene, Non-viral gene therapy for osteoarthritis, Front. Bioeng. Biotechnol. 1 (2021) 618399, https://doi.org/10.3389/fbioe.2020.618399.

[10] F. Colella, J.P. Garcia, M. Sorbona, A. Lolli, B. Antunes, D. D'Atri, F.P.Y. Barré, J. Oieni, M.L. Vainieri, L. Zerrillo, et al., Drug delivery in intervertebral disc degeneration and osteoarthritis: selecting the optimal platform for the delivery of disease-modifying agents, J. Controlled Release 328 (2020) 985–999, https://doi.org/10.1016/j.jconrel.2020.08.041.

[11] C.R. DeJulius, B.L. Walton, J.M. Colazo, R. d'Arcy, N. Francini, J.M. Brunger, C. L. Duvall, Engineering approaches for RNA-based and cell-based osteoarthritis therapies, Nat. Rev. Rheumatol. 20 (2024) 81–100, https://doi.org/10.1038/s41584-023-01067-4.

[12] H. Aini, K. Itaka, A. Fujisawa, H. Uchida, S. Uchida, S. Fukushima, K. Kataoka, T. Saito, U. Chung, S. Ohba, Messenger RNA delivery of a cartilage-anabolic transcription factor as a disease-modifying strategy for osteoarthritis treatment, Sci. Rep. 6 (2016) 18743, https://doi.org/10.1038/srep18743.

[13] A. Kucharski, A. Hollenberg, H. Pan, S. Wickline, C.T. Pham, A. McAlinden, J. Shen, R. O'Keefe, Nanoparticle based Dnmt3b gene therapy attenuates arthritis progression in a murine injury model, OsteoArthritis Cartilage 31 (2023) 695–696, https://doi.org/10.1016/j.joca.2023.02.040.

[14] H. Yan, Y. Hu, A. Akk, M.F. Rai, H. Pan, S.A. Wickline, C.T.N. Pham, Induction of WNT16 via peptide-mRNA nanoparticle-based delivery maintains cartilage homeostasis, Pharmaceutics. 12 (2020) 73, https://doi.org/10.3390/pharmaceutics12010073.

[15] J. Deng, Y. Fukushima, K. Nozaki, H. Nakanishi, E. Yada, Y. Terai, K. Fueki, K. Itaka, Anti-inflammatory therapy for temporomandibular joint osteoarthritis using mRNA medicine encoding interleukin-1 receptor antagonist, Pharmaceutics. 14 (2022) 1785, https://doi.org/10.3390/pharmaceutics14091785.

[16] S. Brown, S. Kumar, B. Sharma, Intra-articular targeting of nanomaterials for the treatment of osteoarthritis, Acta Biomater. 93 (2019) 239–257, https://doi.org/10.1016/j.actbio.2019.03.010.

[17] A.J. Sophia Fox, A. Bedi, S.A Rodeo, The Basic science of articular cartilage: structure, composition, and function, Sports Health 1 (2009) 461, https://doi.org/10.1177/1941738109350438.

[18] C.D. DiDomenico, M. Lintz, L.J. Bonassar, Molecular transport in articular cartilage — What have we learned from the past 50 years? Nat. Rev. Rheumatol. 14 (2018) 393–403, https://doi.org/10.1038/s41584-018-0033-5.

[19] A.P. Pontes, T.J.M. Welting, J. Rip, L.B. Creemers, Polymeric nanoparticles for drug delivery in osteoarthritis, Pharmaceutics. 14 (2022) 2639, https://doi.org/10.3390/pharmaceutics14122639.

[20] J. Wen, H. Li, H. Dai, S. Hua, X. Long, H. Li, S. Ivanovski, C. Xu, Intra-articular nanoparticles based therapies for osteoarthritis and rheumatoid arthritis management, Mater. Today Bio 19 (2023) 100597, https://doi.org/10.1016/j.mtbio.2023.100597.

[21] U. von Mentzer, T. Selldén, L. Råberg, G. Erensoy, A.K. Hultgård Ekwall, A. Stubelius, Synovial fluid profile dictates nanoparticle uptake into cartilage - implications of the protein corona for novel arthritis treatments, OsteoArthritis Cartilage 30 (2022) 1356–1364, https://doi.org/10.1016/j.joca.2022.07.002.

[22] S. Brown, J. Pistiner, I.M. Adjei, B. Sharma, Nanoparticle properties for delivery to cartilage: the implications of disease State, synovial fluid, and off-target uptake, Mol. Pharm. 16 (2019) 469–479, https://doi.org/10.1021/acs.molpharmaceut.7b00484.

[23] A.P. Pontes, S. van der Wal, K. Roelofs, A. Grobbink, L.B. Creemers, J.F. J. Engbersen, J. Rip, A poly(Amidoamine)-based polymeric nanoparticle platform for efficient in vivo delivery of mRNA, Biomater. Adv. 156 (2024) 213713, https://doi.org/10.1016/j.bioadv.2023.213713.

[24] G. Hardenberg, C. Brouwer, R.van Gemerden, N.J. Jones, A.C. Marriott, J. Rip, Polymeric nanoparticle-based mRNA vaccine is protective against influenza virus infection in ferrets, *Mol. Ther. - Nucleic Acids* (2024) 35, https://doi.org/10.1016/j.omtn.2024.102159.

[25] A.P. Pontes, S. van der Wal, S.R. Ranamalla, K. Roelofs, I. Tomuta, L.B. Creemers, J. Rip, Cell uptake and intracellular trafficking of bioreducible poly(Amidoamine) nanoparticles for efficient mRNA translation in chondrocytes, Front. Bioeng. Biotechnol. (2023) 11, https://doi.org/10.3389/fbioe.2023.1290871.

[26] X. Hou, T. Zaks, R. Langer, Y. Dong, Lipid nanoparticles for mRNA delivery, Nat. Rev. Mater. 6 (2021) 1078–1094, https://doi.org/10.1038/s41578-021-00358-0.

[27] C. Lin, Z. Zhong, M.C. Lok, X. Jiang, W.E. Hennink, J. Feijen, J.F.J. Engbersen, Linear poly(Amido Amine)s with secondary and tertiary amino groups and variable amounts of disulfide linkages: synthesis and in vitro gene transfer properties, J. Controlled Release 116 (2006) 130–137, https://doi.org/10.1016/J.JCONREL.2006.09.009.

[28] J.K. Natarajan, J.N. Alumasa, K. Yearick, K.A. Ekoue-Kovi, L.B. Casabianca, A.C. De Dios, C. Wolf, P.D. Roepe, 4-N-, 4-S-, and 4-O-chloroquine analogues: influence of side chain length and quinolyl nitrogen pKa on activity vs chloroquine resistant malaria, J. Med. Chem. 51 (2008) 3466–3479, https://doi.org/10.1021/jm701478a.

[29] N. Araújo-Gomes, G. Zambito, C. Johnbosco, I. Calejo, J. Leijten, C. Löwik, M. Karperien, L. Mezzanotte, L.M. Teixeira, Bioluminescence imaging on-chip platforms for non-invasive high-content bioimaging, Biosens. Bioelectron. 237 (2023) 115510, https://doi.org/10.1016/j.bios.2023.115510.

[30] V. Krenn, L. Morawietz, G.-R. Burmester, R.W. Kinne, U. Mueller-Ladner, B. Muller, T. Haupl, Synovitis score: discrimination between chronic low-grade and high-grade Synovitis, Histopathology 49 (2006) 358–364, https://doi.org/10.1111/j.1365-2559.2006.02508.x.
[31] M. Falahati, F. Attar, M. Sharifi, T. Haertlé, J.-F. Berret, R.H. Khan, A.A. Saboury, A health concern regarding the protein corona, aggregation and disaggregation, *Biochim. Biophys. Acta BBA - Gen. Subj* 1863 (2019) 971–991, https://doi.org/10.1016/j.bbagen.2019.02.012.
[32] C. He, Y. Hu, L. Yin, C. Tang, C. Yin, Effects of particle size and surface charge on cellular uptake and biodistribution of polymeric nanoparticles, Biomaterials 31 (2010) 3657–3666, https://doi.org/10.1016/j.biomaterials.2010.01.065.
[33] X. Zhang, G. Ma, W. Wei, Simulation of nanoparticles interacting with a cell membrane: probing the structural basis and potential biomedical application, NPG. Asia Mater. 13 (2021) 1–18, https://doi.org/10.1038/s41427-021-00320-0.
[34] S. Behzadi, V. Serpooshan, W. Tao, M.A. Hamaly, M.Y. Alkawareek, E.C. Dreaden, D. Brown, A.M. Alkilany, O.C. Farokhzad, M. Mahmoudi, Cellular uptake of nanoparticles: journey inside the cell, Chem. Soc. Rev. 46 (2017) 4218–4244, https://doi.org/10.1039/c6cs00636a.
[35] R. Augustine, A. Hasan, R. Primavera, R.J. Wilson, A.S. Thakor, B.D. Kevadiya, Cellular uptake and retention of nanoparticles: insights on particle properties and interaction with Cellular components, Mater. Today Commun. 25 (2020) 101692, https://doi.org/10.1016/j.mtcomm.2020.101692.
[36] R. Liu, W. Jiang, C.D. Walkey, W.C.W. Chan, Y. Cohen, Prediction of nanoparticles-cell association based on corona proteins and physicochemical properties, Nanoscale 7 (2015) 9664–9675, https://doi.org/10.1039/C5NR01537E.
[37] K.A. Muenzebrock, F.Y.W. Ho, A.P. Pontes, C. Jorquera-Cordero, L. Utomo, J. P. Garcia, P.C. Willems, T.J.M. Welting, J. Rip, L.B. Creemers, Polymeric nanoparticles enable mRNA transfection and its translation in intervertebral disc and Human joint cells, except for M1 macrophages, Pharmaceutics. 16 (2024) 438, https://doi.org/10.3390/pharmaceutics16040438.
[38] X. Li, B. Dai, J. Guo, L. Zheng, Q. Guo, J. Peng, J. Xu, L. Qin, Nanoparticle–Cartilage interaction: pathology-based intra-articular drug delivery for osteoarthritis therapy, Nano-Micro Lett. 13 (2021) 149, https://doi.org/10.1007/s40820-021-00670-y.
[39] H.K. Vincent, S.S. Percival, B.P. Conrad, A.N. Seay, C. Montero, K.R. Vincent, Hyaluronic acid (HA) viscosupplementation on synovial fluid inflammation in knee osteoarthritis: A pilot study, Open. Orthop. J. 7 (2013) 378–384, https://doi.org/10.2174/1874325001307010378.
[40] X.-L. Xu, Y. Xue, J.-Y. Ding, Z.-H. Zhu, X.-C. Wu, Y.-J. Song, Y.-L. Cao, L.-G. Tang, D.-F. Ding, J.-G. Xu, Nanodevices for deep cartilage penetration, Acta Biomater. 154 (2022) 23–48, https://doi.org/10.1016/j.actbio.2022.10.007.
[41] A. Petit, E.M. Redout, C.H. van de Lest, J.C. de Grauw, B. Müller, R. Meyboom, P. van Midwoud, T. Vermonden, W.E. Hennink, P. René van Weeren, Sustained intra-articular release of Celecoxib from *in situ* forming gels made of acetyl-capped PCLA-PEG-PCLA triblock copolymers in horses, Biomaterials 53 (2015) 426–436, https://doi.org/10.1016/j.biomaterials.2015.02.109.